Hydrothermal equalibria and ore formation

Alekseyev V.A., Burmistrov A.A., Gromiak I.N. Quartz dissolution in water vapor and solution distillation in quartz–water–vapor system at 300°C

Vernadsky Institute of Geochemistry and Analytical Chemistry RAS, Moscow (alekseyev-v@geokhi.ru)

Abstract. Experiments were performed with quartz crystals and water at 300°C and small temperature gradients. In experiments where the crystal was located in vapor phase, the rate constant of quartz dissolution for vapor was measured for the first time, which was 630 times less than for water. Calculations have shown that the time to reach the equilibrium of quartz with water and vapor is equally short (2-3 days), but the subsequent quartz recrystallization in vapor is 2 orders of magnitude slower than in water. When the crystal was located in both water and vapor, the dissolution of stable quartz in water led to the deposition of metastable opal on the quartz in vapor. This unusual phenomenon is caused by changes in properties of fluid when its size decreases, i.e. it belongs to the field of nanogeochemistry. In particular, it is explained by distillation caused by the predominant evaporation of a thin layer of solution on quartz. Evaporation increased in the presence of grooves and rough surfaces. The process was 3.5 orders of magnitude faster than recrystallization, since the system was further from equilibrium. Distillation can be the cause of asymmetry of natural crystallization cavities, lower parts of which were dissolved, and minerals were deposited onto upper parts.

Keywords: *quartz, opal, transformation, water–vapor interface, distillation*

INTRODUCTION Quartz (α-quartz) is stable up to at least 573°C and 20 kbar (Dove, 1995). Opal is formed from supersaturated solutions in the stability region of quartz, i.e. is a metastable mineral and, with time, transforms into quartz (Bettermann and Liebau, 1975). Recently, we discovered the reverse transformation of quartz into opal caused by the distillation of a solution (Alekseyev and Medvedeva, 2018). In this paper, we attempted to carry out such a transformation under conditions more real for nature by replacing the platinum wall with the quartz crystal itself. This can serve as convincing evidence that the observed phenomenon is not an exclusively experimental artifact.

METHODS In the experiments, bidistilled water and natural quartz crystals were used, which were purified from impurities by repeated boiling in HCl and H_2O. In autoclaves, crystals were fixed with wire mountings in the desired position (Fig. 1). The autoclaves of each series were heated in pairs on top of each other at 300±2°C. On the surface of the lower and upper autoclave, the bottom-up temperature slightly increased and decreased: 0.15 and -0.08 °/cm, respectively (Alekseyev, Medvedeva, 2018). After the experiments, the autoclaves were quenched, the solutions were filtered and analyzed for Si (ICP-AES). Newly formed silica was studied using an endoscope, X-ray diffraction, and an optical and scanning electron microscope. New to this kind of research was 3d scanning of crystals. The measured SiO_2 concentrations in quenching solutions were recalculated to the temperature of experiments taking into account dilution of solutions with condensate during quenching (Verma, 2000).

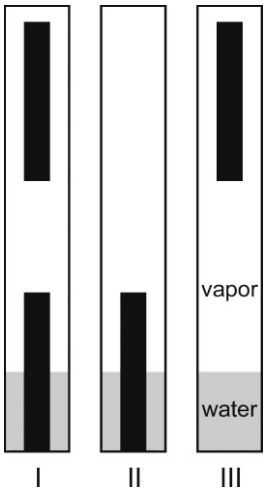

Fig. 1. The position of quartz crystals in autoclaves in the series of experiments I, II, III.

RESULTS

Series I. Despite the long duration of the experiments, the silica concentrations in water (m_w) (Tab. 1) were lower than the solubility of quartz at 10.6 mmol/kg (Plyasunov, 2012). The mass loss of the upper crystals (in vapor) was negligible, and for the lower crystals, it was greater and exceeded the mass of dissolved silica (M_1). This is due to the deposition of solid silica (M_2) on the walls of the autoclaves at the level of the water surface. According to X-ray diffraction, this silica is cristobalite-tridymite opal. In addition, opal was deposited on one of the faces of the lower crystal above the water level (Fig. 2).

Series II. The solution remained undersaturated relative to quartz despite the increase in the duration of the experiments compared to series I (Tab. 1). The creation of a rough quartz surface changed the mechanism of deposition of opal, which formed a rim in the middle part of the crystal, where the water–vapor interface was located (Fig. 3).

Series III. In three experiments where opal was not formed, the rate constant of the dissolution of quartz in saturated water vapor was measured. In this case, the equation of the rate of dissolution of quartz in water was used (Rimstidt, Barnes, 1980):

$$k_v = -\frac{m_{w,eq} M_w}{St} \log\left(1 - \frac{m_w}{m_{w,eq}}\right) \quad (1)$$

where m_w and $m_{w,eq}$ is the actual and equilibrium concentration of silica in water, t is time, S is the surface area of quartz, k_v is the rate constant of dissolution of quartz in steam, and M_w is the mass of water. The applicability of equation (1) to the dissolution of quartz in vapor is justified by two circumstances (Plyasunov, 2012): 1) in water and vapor, silica is represented by species of the same type $Si(OH)_4^0$, 2) a low equilibrium ratio $\kappa = m_v / m_w = 0.0047$ means that almost all silica transferred from quartz to steam then passed into water and accumulated there. Calculations at $M_w = 0.0043$ kg, $m_{w,eq} = 0.0106$ mol/kg, m_w, t, S from the table 1 yielded $k_v = 2.7\times10^{-9}$ mol m^{-2} s^{-1}, which is 630 times less than the same constant for water (Tester et al., 1994). Given that $m_v / m_{v,eq} = m_w / m_{w,eq}$, the differential equation for the dissolution rate of quartz in vapor has the form:

$$r = \frac{dn}{Sdt} = k_v\left(1 - \frac{m_w}{m_{w,eq}}\right) \quad (2)$$

where n is the number of dissolved moles of the mineral. The calculated dependence of r on the degree of saturation of the solution is in good agreement with the experimental values of r obtained near equilibrium and far from it (Fig. 4), which confirms the identical form of the equation for water

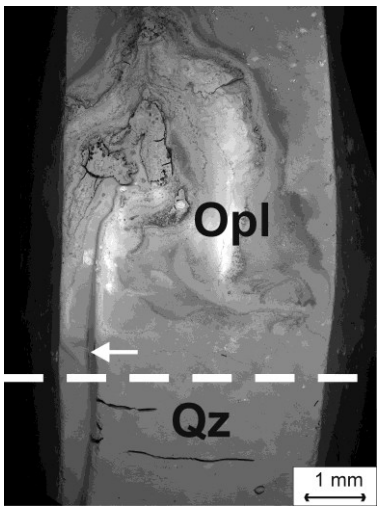

Fig. 2. SEM-photo of a quartz crystal (Qz) with an opal (Opl) deposited on it in series I. The dotted line shows the water–vapor boundary. The arrow shows the groove where the solution was raised.

Fig. 3. Diagram of size deviations between combined 3d models of a quartz crystal obtained before and after the interaction of quartz with water (series II). The light rim shows a local increase in the size of the crystal to 0.1 mm due to the deposition of opal on quartz at the water–vapor boundary.

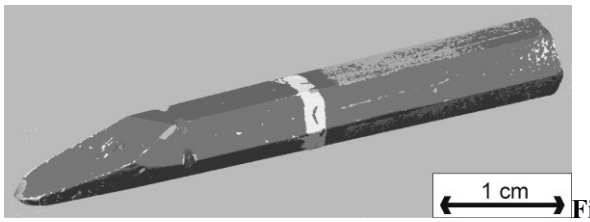

Table 1. The conditions and results of experiments with water (6 g) and quartz crystals at 300°C: location of autoclave in furnace and crystals in autoclave, crystal mass (M_c), heating time (t), silica concentration in water (m_w) mass loss of crystal (ΔM_c), silica mass in solution (M_1) and in new solid phase (M_2), surface area (S) and volume (V) of crystal.

Location		M_c	t	m_w	Silica mass balance, mg				S	V
auto-clave	crystal	g	days	mmol/kg	ΔM_c	M_1	M_2	Σ	cm^2	cm^3
Series I: two quartz crystals, at the top and bottom of the autoclave										
top	top	7.028	42	8.25	-0.8	3.0	9.0	-13.2		
	bottom	8.552			-24.4					
bottom	top	6.428	42	6.29	-1.1	2.2	9.0	-8.2		
	bottom	7.850			-18.3					
Series II: one quartz crystal at the bottom of the autoclave										
top	bottom	7.049	77	7.87	-2.1	2.0	0	-0.1	14.38	2.671
bottom	bottom	4.524	77	7.37	-6.0	1.9	4.0	-0.1	11.38	1.723
Series III: one quartz crystal at the top of the autoclave										
top	top	7.849	77	5.98	-0.9	1.5	0	0.6	16.19	2.987
bottom	top	8.260	77	2.29	-0.8	0.6	0*	-0.2	16.33	3.143
top	top	7.348	7.9	0.661	0.1	0.2	0	0.3	15.93	2.796
bottom	top	7.202	7.9	0.630	-1.4	0.2	0	-1.2	15.78	2.753

* a thin white ring of opal (fractions of mg) was on the wall at the water–vapor interface

and vapor.

DISCUSSION

Traditional approach. To calculate the time required to reach the quartz–water and quartz–vapor equilibrium, we use equation (1) in the form:

$$t = -\frac{m_{eq} M}{kS} \ln\left(1 - \frac{m}{m_{eq}}\right) \quad (3)$$

where all values refer to either water or vapor. We believe that equilibrium is reached if $m = 0.99 m_{eq}$. In the calculations, we will follow the experimental scheme of series II (Tab. 1, Fig. 1), when one half of the crystal (S = 6.4 cm^2) was dissolved in water (M = 4.3 g) and the other in vapor (M = 1.7 g). The calculations gave close values of t for water and vapor, equal to 2.2 and 2.7 days, respectively. This proximity is explained by the fact that a smaller value of k for vapor in the denominator is compensated by lower values of m_{eq} and M in the numerator.

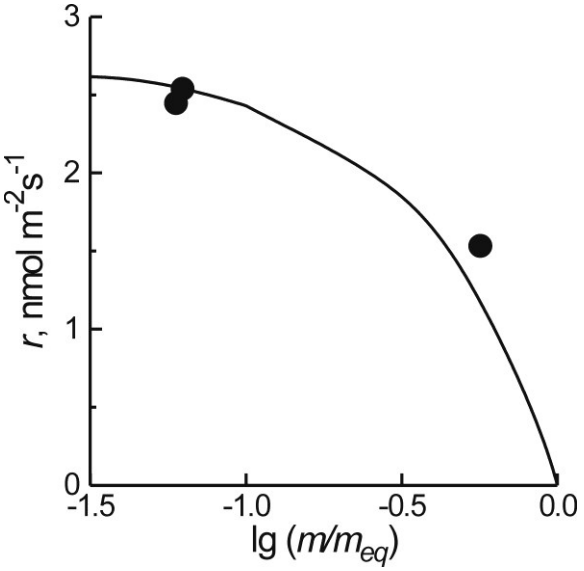

Fig. 4. The rate of dissolution of quartz in water vapor (r) depending on the degree of saturation of the vapor with silica (m/m_{eq}). Line is the result of calculation by equation (2) at k_v = 2.7 nmol m^{-2} s^{-1}, symbols are experimental data (series III).

After reaching a state close to equilibrium, quartz recrystallization should begin if at least a small temperature gradient exists. We simulate this process for series II, when the water–vapor boundary has a temperature of 300°C, and the temperature of the bottom and top of the crystal (T_1 and T_2) is 300 + 0.24 and 300 – 0.24 °C in the upper autoclave, 300 – 0.45 and 300 + 0.45 °C in the lower one. The recrystallization rate is equal to the rate of dissolution (deposition) of quartz in water (left) or in vapor (right):

$$r = k_w S_w \left(1 - \frac{m_w}{m_{w,eq}}\right) = -k_v S_v \left(1 - \frac{m_v}{m_{v,eq}}\right) \quad (4)$$

Since $m_v = \kappa m_w$, both rates affect each other. As a result, a steady state of the reaction is established with a constant value of m_w, which can be calculated from equality (4). This value was substituted into equation (4) and the value of r was calculated. The calculations were performed for a wide range of values T_1 and T_2, not only for water–vapor media, but also for single-phase media, water and vapor. The calculated rate of quartz recrystallization increases with increasing temperature differences, but it is lower for the vapor medium than for the water medium by ~2 orders of magnitude, and even lower for the water–vapor medium by ~0.5 orders of magnitude (Fig. 5). Thus, according to the traditional approach, in this system, you can expect only rapid (for 2-3 days) saturation of water with silica and subsequent slow (experimentally almost undetectable) recrystallization of quartz. However, in fact, we observe a completely different picture: the rapid transformation of stable quartz into metastable opal (according to figure 5, ~3.5 orders of magnitude faster than simple recrystallization of quartz), but the m_w value remains below the solubility of quartz.

Distillation of the solution. An alternative approach is based on changing the properties of particles and fluids as their sizes decrease, when the contribution of surface energy becomes noticeable (Alekseyev, 2019). In particular, a thin (less than 100 nm) film of liquid at the edge of the meniscus becomes more thermally conductive than in the volume, which ensures its higher evaporation rate (Plawsky et al., 2008). In a closed system with hydrophilic walls, this can lead to spontaneous distillation of the solution, which means gradual replacement of the solution with condensate (Alekseyev et al., 2018). The supersaturation required for opal deposition was achieved by evaporation of the solution in the film. Under the action of capillary forces, the solution film is able to rise along grooves and rough surfaces (Bico et al., 2002), increasing the evaporation area and, consequently, the distillation rate (Alekseyev et al., 2019). For example, the natural groove on quartz (the arrow in Fig. 2) contributed to the rapid rise of the solution, which spread along the face and evaporated, depositing the opal in the form of scattered sinter forms. Compact deposition of opal was observed on a rough surface that provided a high rate of evaporation (Fig. 3).

In nature, there is often an asymmetry of crystallization cavities (large crystals at the top), which is explained by the growth of the upper crystals due to the dissolution of the lower ones (Askhabov, 1993). Distillation of the solution may be the mechanism that causes this recrystallization. Its distinctive feature is the renewal of the solvent capacity of the solution. Therefore, the cavity has the ability to migrate down due to the constant

dissolution of its bottom. As a result, a small volume of the solution can cause phase transformations in a large volume of rock.

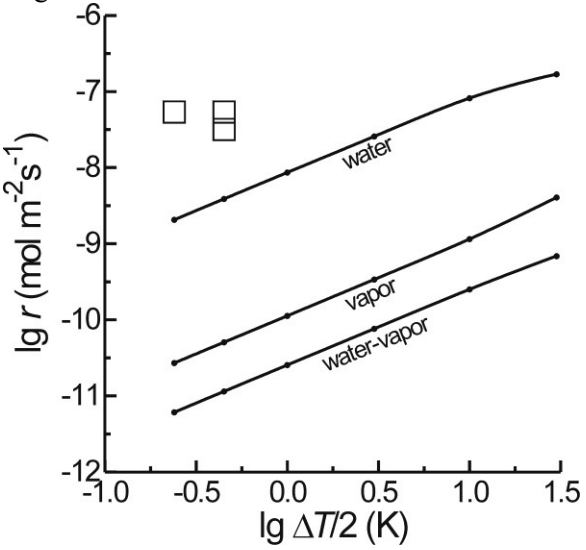

Fig. 5. The rate of quartz dissolution (r) during its recrystallization, depending on the temperature difference (ΔT) between the top and bottom of the quartz crystal for water, vapor, and water-vapor media. Lines are the results of calculation by equation (4), symbols are experiments on the transformation of quartz into opal (series I and II)

References:

Alekseyev V.A. Nanoparticles and nanofluids in water–rock interactions // Geochem. Int. 2019. Vol. 57. № 4. P. 357-368.

Alekseyev V.A., Medvedeva L.S. Silica distribution in the system quartz–water–vapor depending on the temperature gradient // Geochem. Int. 2018. Vol. 56. № 2. P. 136-147.

Alekseyev V.A., Medvedeva L.S., Balashov V.N., Burmistrov A.A., Gromyak I.N. Experimental study of unequilibrated silica transfer from liquid water to the vapor phase // Geochem. Int. 2018. Vol. 56. № 7. P. 617-627.

Alekseyev V., Balashov V., Medvedeva L., Opolchentsev A. Spontaneous distillation of silica-bearing solution in closed system with rough walls // E3S Web of Conferences. 2019. Vol. 98. 04001.

Ashabov A.M. Crystal genesis and evolution of "crystal-environment" system. Saint-Petersburg: Nauka, 1993. 154 p. (in Russian).

Bettermann P., Liebau F. The transformation of amorphous silica to crystalline silica under hydrothermal conditions // Contrib. Mineral. Petrol. 1975. Vol. 53. P. 25-36.

Bico J., Thiele U., Quéré D. Wetting of textured surfaces // Colloids and Surfaces A. 2002. Vol. 206. P. 41-46.

Dove P.M. Kinetic and thermodynamic controls on silica reactivity in weathering environments // Rev. Mineral. 1995. Vol. 31. P. 235-290.

Plawsky, J.L., Ojha, M., Chatterjee, A., Wayner Jr., P.C. Review of the effects of surface topography, surface chemistry, and fluid physics on evaporation at the contact line // Chem. Engin. Commun. 2008. Vol. 196. P. 658-696.

Plyasunov A.V. Thermodynamics of $Si(OH)_4$ in the vapor phase of water: Henry's and vapor–liquid distribution constants, fugacity and cross virial coefficients // Geochim. Cosmochim. Acta. 2012. Vol. 77. P. 215-231.

Rimstidt J.D., Barnes H.L. The kinetics of silica–water reactions // Geochim. Cosmochim. Acta. 1980. Vol. 44. № 11. P. 1683-1699.

Tester J.W., Worley W.G., Robinson B.A., et al. Correlating quartz dissolution kinetics in pure water from 25 to 625°C // Geochim. Cosmochim. Acta. 1994. Vol. 58. № 11. P. 2407-2420.

Verma M.P. Chemical thermodynamics of silica: a critique on its geothermometer // Geothermics. 2000. Vol. 29. P. 323-346.

Balitsky V.S., Balitskaya L.V., Golunova M.A., Setkova T.V., Bublikova T.M. New experimental data on phase transformations and states of synthetic water-hydrocarbon inclusions in quartz

IEM RAS, Chernogolovka (balvlad@iem.ac.ru)

Abstract. A new series of experiments was carried out on the interaction of aqueous solutions with oil and various bituminous rocks in the temperature range of 240-670 °C and pressures of 5-150 MPa. Simultaneously, in the same experiments, quartz was grown with fluid, mainly water-hydrocarbon inclusions. As a result of studying these inclusions by methods of thermobarogeochemistry, a variety of phase compositions and states of water-hydrocarbon fluids, including their homogeneous states, were established. This confirms the opinion that water-hydrocarbon fluids are found on depths of 20-25 km in a homogeneous state.

Keywords: water-hydrocarbon inclusions, oil, quartz synthesis, oil phase composition, phase transformations, supercritical fluids, thermobarogeochemistry

Introduction. Hydrothermal solutions in the Earth's interior almost always come into contact and interact with crude oil. The nature of such interactions at elevated and high temperatures and pressures is still insufficiently studied. This especially applies to the phase composition and states of oil located at depths of more than 5–10 km at temperatures of 150–290°C and pressures of tens of megapascals. A further depths increase during the search, exploration and oil production more complicates the predictions regarding phase composition and especially the oil states in the Earth's interior. Without these data, it is also impossible to solve some questions of the oil genesis and oil secondary replenishment in the abandoned fields. Modeling experimental studies based on visualization of the processes occurring during heating and cooling of synthetic water-hydrocarbon inclusions in quartz grown simultaneously with the interaction of oil with hydrothermal solutions are promising in this case.

Approaches, methods, equipment and materials. The presented work provides generalized experimental data on the establishment of the phase

composition and states of oil in synthetic water-hydrocarbon inclusions formed in quartz grown in hydrothermal, including sub- and supercritical solutions at temperatures of 240 – 550°C (single experiments - up to 700°C) and saturated steam pressures and above (up to 150 MPa). The possibility of direct (in situ) determination of both the phase composition and the states of water-oil systems at elevated and high temperatures and pressures is an advantage of the chosen approach. The study of fluid inclusions was carried out using the methods of modern thermobarogeochemistry (Ermakov,1972; Roedder, 1984), in particular using the most informative microthermometry, conventional and fluorescence microscopy, local, including high-temperature (up to 400°C) Fourier IR- and Raman-spectroscopy, as well as gas-liquid chromatography (Balitsky et al., 2011; 2014).

The experiments were performed mainly with crude oil from the Bavlinskoye field (Tatarstan). The oil was subjected to heat treatment in autoclaves with a volume of 30 to 280 ml, made of heat-resistant stainless steel and Cr – Ni alloy, designed to operate at temperatures up to 500 and 700°C and pressures up to 100 and 150 MPa, respectively. The autoclaves were heated in electric high furnace. Temperature control and regulation was carried out using standard thermal measuring devices (TYP 01 T4, TYP R3, Thermodat-25M1). The temperature measurement accuracy was ± 3°C. The pressure was estimated by the PVT diagrams for the initial aqueous solutions (Samoilovich, 1969). At first the autoclaves were loaded with quartz mixture and seed ZY- and ZX-plates with 2-4 mm thick, 4-8 mm wide and 140-200 mm long, then they were filled with one of the initial aqueous solutions (3, 5 and 10 wt% $NaHCO_3$ or 0.5, 2, and 4 wt% Na_2CO_3) and then crude oil. The required pressure was set by the autoclave filling factors of the solutions. The volume of the poured oil was varied from tenths to 70-85 vol. % in relation to the volume of aqueous solution. The experiments duration was mainly 20-30 days, but in a number of control experiments it decreased to several days or increased to 100-200 days. The preparation of equipment and materials for experiments was discussed in detail in our earlier publications (Balitsky et al., 2011; 2014; 2016). Examples of synthetic water-hydrocarbon inclusions in quartz crystals are shown in the photographs (Fig. 1).

Results. The main results on the determination of

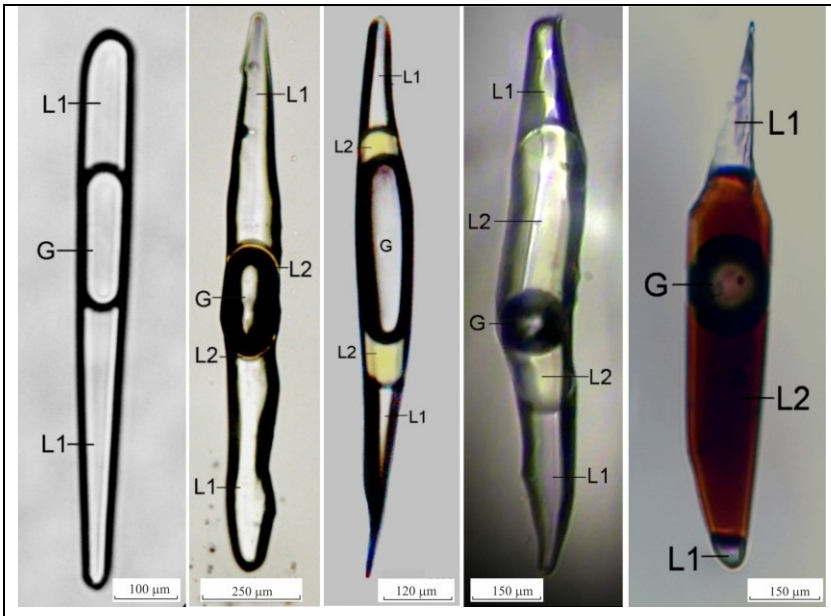

Fig. 1. Morphology and phase composition of water-hydrocarbon inclusions in quartz grown at relatively low (240/310 ºC) temperatures and pressures (5–12 MPa) in heterogeneous weakly alkaline aqueous solutions (3, 5, and 10 wt% $NaHCO_3$) in the presence of oil (2 - 50 vol.%).

Here and below the phases: L1 - aqueous solution, L2 - liquid hydrocarbons, G - gaseous hydrocarbons (mainly methane).

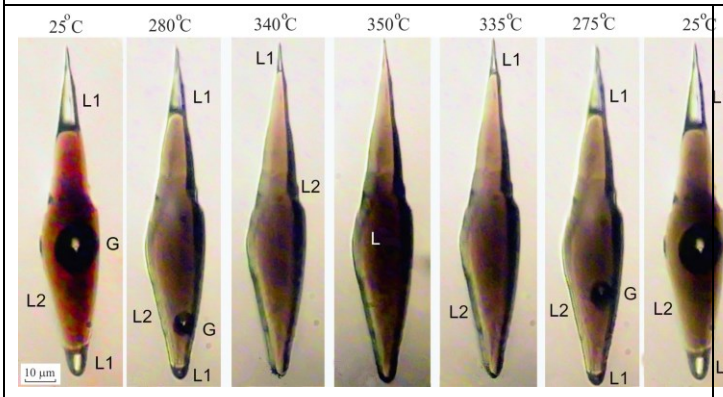

Fig. 2. Microthermogram fragment of a substantially oil inclusions in synthetic quartz grown by the interaction of oil with a hydrothermal solution.

The phase ratio under room conditions is characterized by the inequality L2> G> L1. At the inclusions heating, the gas phase disappears at the beginning at 340 ºC and the inclusions become two-phase with the phase ratio L2 >> L1. Then at 350 ºC, the aqueous phase L1 completely dissolved in oil L2 with the transition of inclusion into a homogeneous stage. The sequential restoration of all disappeared phases and their states during cooling occurs.

the phase composition and state of inclusions at elevated and high temperatures and pressures are demonstrated in microthermograms (Fig. 2–4), compiled based on videos taken in high-temperature chambers.

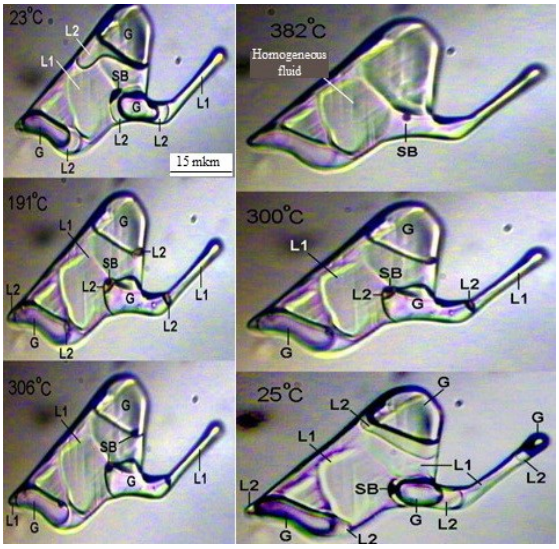

Fig. 3. Reversible change in the phase composition and states of a high-temperature water-hydrocarbon inclusion in the temperature range 23 °C – 382 °C – 25 °C. The volumetric ratio of the phases under normal conditions is L1> G≈L2 >> SB (where SB is solid bitumen, its proportion practically does not change over the all temperature range). Liquid hydrocarbons dissolve completely at the inclusion heats up to 306 ° C with transition to a two-phase gas-liquid (L1≈G) state. At 382 ° C, the gas phase (mainly methane) disappears with the transition of the inclusion into a homogeneous state. The inclusion completely returns to the intermediate and initial phase compositions and states at cooling.

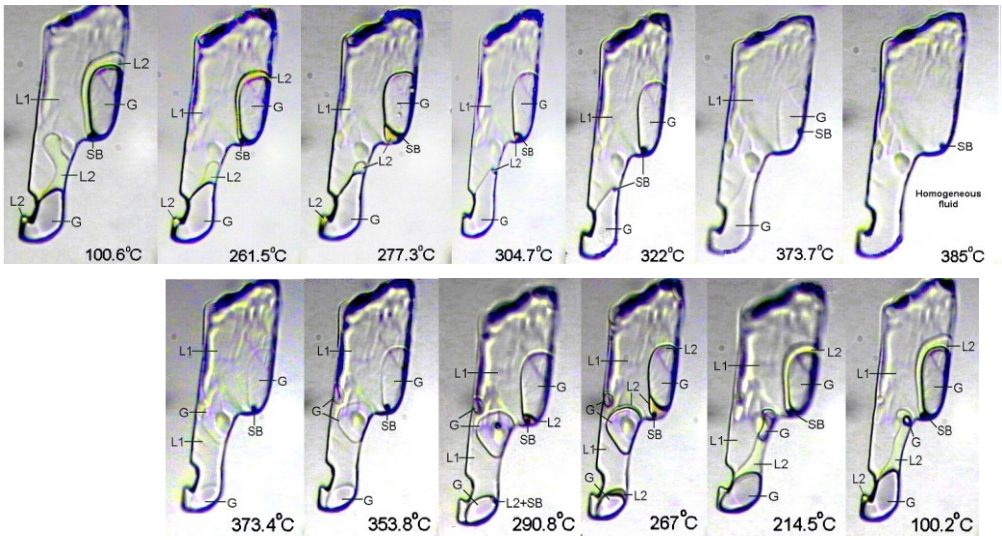

Fig. 4. Change in the phase composition and state of the high-temperature water-hydrocarbon inclusion with the volumetric ratio of phases L1> G> L2 >> SB during heating and cooling. The phase of solid bitumen (SB) remains practically unchanged in the all temperature range. Below 100°C - the changes are insignificant and up to 322°C the inclution retains the three-phase (taking into account the SB phase - four-phase) state. The liquid hydrocarbon phase disappears (dissolves) at 322°C and the fluid transforms into a two-phase gaseous liquid state. A further temperature increase to 385°C leads to complete homogenization of the fluid with the disappearance of the gas phase (mainly methane).

After repeated autoclave heat treatment of the inclusions for 15 days at various temperatures, an unexpected and interesting result was obtained. After treatment at 300°C, the phase composition and volumetric phase ratios in the inclusions remain unchanged. However, at 320°C, the methane, CO_2 and residual solid bitumen appear in inclusion. Light fractions proportion also increases. The temperature increase to 350 and 380°C leads to the gradual disappearance of liquid hydrocarbons and the aqueous phase with a simultaneous increase in methane, carbon dioxide and solid bitumen proportion. This was fixed in many experiments. Moreover, in experiments at temperatures of 450–500°C and pressures of 100–120 MPa, complete disappearance of liquid hydrocarbons with their transformation into solid bitumens and methane was noted in such inclusions. In addition, at 670°C, the solid bitumens transform to crystalline graphite according to Raman spectra.

Conclusion. The analysis of microthermograms with the determination of the phase composition and

states of the inclusions demonstratively proves the existence of various types of water-hydrocarbon fluids in the Earth's interior. The main ones are:

- heterogeneous three-phase fluids with volumetric phase ratios: L1> G >> L2;
- heterogeneous two-phase liquid water-hydrocarbon fluids with phase ratio L2 >> L1 with completely dissolved gas phase G;
- homogeneous liquid, predominantly aqueous fluids $L1_{hom}$ with completely dissolved gaseous and liquid hydrocarbons;
- homogeneous gas fluids G_{hom} with completely dissolved phases of liquid hydrocarbons and water;
- homogeneous liquid hydrocarbon fluids $L2_{hom}$ with completely dissolved water (L1) and gas (HC) phases.

The work was carried out in IEM RAS, research project AAAA-A18-118020590150-6.

References

Balitsky, V. S.; Penteley, S. V.; Balitskaya, L. V.; Novikova, M. A.; Bublikova, T. M. Visual In-Situ Monitoring of the Behavior and Phase States of Water-Hydrocarbon Inclusions at High Temperatures and Pressures // Petrology. 2011. V. 19. Iss. 7. P. 653-674.

Balitsky VS, Bondarenko GV, Pironon J, Penteley SV, Balitskaya LV, Golunova MA, Bublikova TM (2014) The causes of vertical zonation in the distribution of hydrocarbons over the Earth's interior: Experimental evidence of the cracking of crude oil in high-temperature water-hydrocarbon fluids. Russian Journal of Physical Chemistry B (8)7: 901-918

Balitsky VS, Penteley SV, Pironon J, Barres O, Balitskaya LV, and Setkova TV (2016) Phase states of hydrous–hydrocarbon fluids at elevated and high temperatures and pressures: Study of the forms and maximal depths of oil occurrence in the earth's interior. Dokl Earth Sci 466(2):130–134

Ermakov NP (1972) Geochemical systems of mineral inclusions. Nedra, Moscow, 376 p

Roedder E (1984) Fluid Inclusions. Rev. Mineral. Mineralogical Society of America, 12, 644 p

Samoilovich LA (1969) Relations between the pressure, temperature, and density of aqueous salt solutions. VNIISIMS, Moscow, 48 p

Bublikova T.M., Setkova T.V., Balitsky V.S. Theoretical study of the solubility of basic copper carbonates in ammonium chloride systems

IEM RAS, Chernogolovka (tmb@iem.ac.ru)

Abstract. The phase formation in the system CuO – CO_2 – H_2O – NH_4Cl was studied for temperature 25 °C, pressure 0.1 MPa and concentrations of ammonium chloride 1.0, 2.0 и 3.0 *m*. Phase relations were studied by calculating and plotting the solubility diagrams of copper compounds in the specified system. The stability fields of tenorite, malachite, azurite, atacamite and compositions of solutions equilibrium with solid phases under specified conditions are determined. The effect of changes in the concentration of ammonium chloride on the copper content in an equilibrium solution with solid phases is shown.

Keywords: phase formation, tenorite, malachite, azurite, atacamite, ammonium chloride-solution, copper leaching, hydrometallurgy

The results of studying the phase formation in the CuO – CO_2 – H_2O – NH_4Cl system are directly related to the items of improving the technology of hydrometallurgical copper extraction. The acid-alkaline leaching methods makes it possible to solve the problems of pyrometallurgical copper production (environmental due to increased heat, dust and gas separation, explosion hazard), as well as to use raw materials more fully, to extract copper from depleted oxidized and native ores and waste from processing primary ores. Hydrometallurgical methods are based on selective leaching of copper-rich minerals, including in ammonia solutions. The extraction ratio of copper ranges from 20 (copper slags of the Balkhash brass works) to 99% (Bwana Mkumba brass works, Zambia), depends on the composition of the ore and the efficiency of the applied technology. Ground copper oxide minerals are treated with an alkaline solution followed by a separation step. The mixtures of ammonium hydroxide with ammonium salts (chloride, sulfate, carbonate) are effective leaching reagent (Nadirov et al., 2017; Xi Wang et al., 2010; Liu Wei et al., 2010).

This study purposes are investigation of phase formation in copper-carbonate systems with ammonium chloride solutions, establish of solid phases stability fields and the effect of ammonium chloride concentration on the solubility of copper compounds. The phase relationships were studied by calculating and plotting the copper compounds solubility diagrams of CuO – CO_2 – H_2O – NH_4Cl system. The HCh software package (Shvarov, Bastrakov, 1999) and thermodynamic properties of substances database were used. This database was formed earlier when calculating the solubility diagrams of the CuO – CO_2 – H_2O – NH_3 system (Bublikova et al., 2000; Bublikova et al., 2013) and additionally includes the thermodynamic properties of chlorine containing solid phases and solution species.

Isothermal diagrams of the solubility of CuO – CO_2 – H_2O – NH_4Cl system for temperature of 25°C, pressure of 0.1 MPa, and 1.0, 2.0, and 3.0 *m* ammonium chloride concentrations are shown in Fig. 1a. The selected NH_4Cl concentrations range corresponds to the salt concentrations used in industrial copper leaching processes.

Only fifteen of more than two hundred copper-bearing minerals have industrial value, including azurite, atacamite, tenorite and malachite - the most

abundant mineral in copper oxide ores. Figure 1a shows that the solid phases of atacamite, tenorite, malachite, azurite, and copper carbonate are stable under the given conditions and have rather wide stability fields. Moreover, atacamite together with tenorite, malachite and azurite is formed in different quantitative ratios, which vary depending on solution concentration and the total acidity in the system (Fig. 1b). In 1.0 *m* NH_4Cl solution, the partial pressure of CO_2 increases and, accordingly, pH of the solution decreases, the atacamite -tenorite ratio does not change and remains constant and equal to 10% ***At*** + 90% ***Ten***. Then the solution acidity increases, the atacamite content decreases: in ***At*** – ***Mal*** stability field from 10 to 0.2% and in ***At*** – ***Az*** field from 0.2% to 0. The quantitative ratios of solid phases in equilibrium with 2.0 *m* NH_4Cl solution are different (see Fig. 1b), but changes character does not shift significantly. The atacamite content decreases from 60% (***At*** – ***Ten***) to 0 (***At*** – ***Az***). An increase in solution concentration to 3.0 m NH_4Cl leads to disappearance of the tenorite stability field and its complete replacement by atacamite under the given thermodynamic conditions.

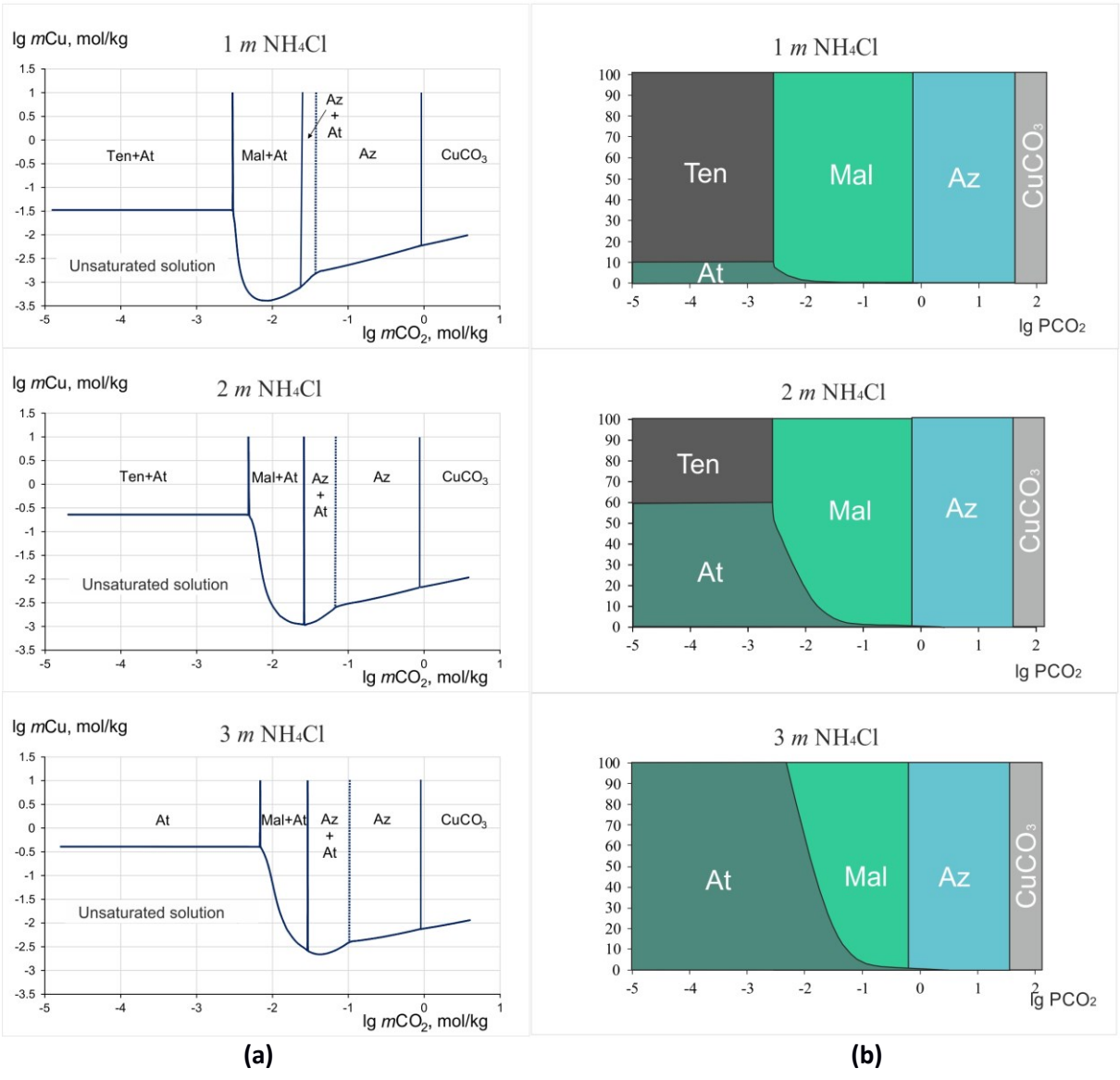

Fig. 1. Diagrams of solubility (a), and stability fields ratio (b) of copper compounds in CuO – CO_2 – H_2O –NH_4Cl system. T = 25 °C; P = 0.1 MPa; NH_4Cl concentration: 1.0, 2.0 and 3.0 *m*. ***At*** – *atacamite,* ***Ten*** – *tenorite,* ***Mal*** – *malachite,* ***Az*** – *azurite.*

In natural conditions, in the oxidation zone of copper-sulfide deposits (in ammonia absence), a process of replacement of atacamite with malachite is observed, often with pseudomorphs formation (Ural, Turinsky mines). The regularities in the calculated equilibrium diagrams are similar. Then concentration of ammonium chloride decreases and partial pressure of CO_2 increases, the atacamite content decreases.

Analysis of the content of the total amount of copper in equilibrium solutions shows that copper content increases with increasing the concentration of ammonium chloride. The total copper concentration is determined by the presence in the solution of mainly copper-ammonia complexes in the form of $Cu(NH_3)_n^{2+}$ and $CuCO_3^0$, $CuHCO_3^+$, $CuCl^-_3$ species. The complex character of the solubility curve in the At - Mal and At - Az regions is associated with the change of species amounts with increasing molar fraction of CO_2 in the solution. The content of copper-ammonia complexes in the solution decreases, and carbonate-bicarbonate species content increases when the shift to a more acidic medium takes place (with pCO_2 increase).

Comparison of obtained results with our previous theoretical calculations and experimental data on malachite solubility in ammonia solutions shows that the equilibrium copper concentrations in the 2.0 and 3.0 *m* NH_4OH solution are higher than in the 2.0 and 3.0 *m* NH_4Cl solutions under the same thermodynamic conditions. However, pure ammonium hydroxide is almost not used in practice, because it slowly dissolves metallic copper and copper oxide. Using the ammonium chloride gives certain advantages over other ammonium salts: 1) copper and other non-ferrous metals form complexes with chloride ions, which are readily soluble in water; 2) chloride is an aggressive ion that improves oxide dissolution kinetics. The results of study of phase formation processes, copper solubility, changes in the composition of equilibrium solutions using thermodynamic modeling, make it possible to understand the reaction of the system to changes that occur during the minerals dissolution, vary the conditions in the development of a specific hydrometallurgical process, and predict the results of the leaching process depending on base ore composition.

The work was carried out in IEM RAS, research project *AAAA-A18*-118020590150-6.

References

Bublikova T.M., Balitsky V.S., Timokhina I.V. Synthesis and main properties of jewelry and ornamental malachite. Synthesis of minerals. V. 1. Alexandrov, VNIISIMS. 2000. 662 p. (In Russian).

Bublikova T.M., Balitsky V.S., Setkova T.V. Study of basic copper carbonate solubility in aqueous ammonia solutions (theoretical and experimental data) // Experiment in GeoSciences. 2013. Vol.19, No.1. P.74 – 75.

Liu Wei, Tang Mo-tang, Tang Chao-bo, Ht Jing, Yang Sheng-hai, Yang Jian-guang. Dissolution kinetics of low grade complex copper ore in ammonia-ammonium chloride solution // Trans. Nonferrous Met. Soc. China. 2010. V. 20. P. 910 – 917.

Nadirov R., Syzdykova L, Zhussupova A. Copper smelter slag treatment by ammonia solution: Leaching process optimization // J. Cent. South Univ. 2017. V. 24. P. 2799 − 2804.

Shvarov Yu.V., Bastrakov E. HCh: a Software Package for Geochemical Equilibrium Modeling: User's Guide (AGSO RECORD 1999/y). Canberra: Austr. Geol. Surv. Organisation; Dept. Industry, Science and Resources. 1999. 57 p.

Xi Wang, Qiyuan Chen, Huiping Hu, Zhoulan Yin, Zhongliang Xiao. Solubility prediction of malachite in aqueous ammoniacal ammonium chloride solutions at 25 °C // Hydrometallurgy. 2009. V. 99. P. 231 – 237.

Korzhinskaya V.S., Kotova N.P. Temperature effect on the behavior of Ta and Nb during the dissolution OF pyrochlore, tantalite, β-Ta_2O_5 and β-Nb_2O_5 in (HF+HCl) solutions.

Institute of Experimental Mineralogy RAS, Chernogolovka Moscow district (vkor@iem.ac.ru, kotova@iem.ac.ru)

Abstract. The solubilities of tantalum and niobium oxides, as well as the natural minerals of pyrochlore $(Ca,Na)_2(Nb,Ta)_2O_6(O,OH,F)$ and tantalite $(Mn,Fe)(Ta,Nb)_2O_6$ in (HF+HCl) mixed fluids were experimentally studied. The data obtained made it possible to estimate the equilibrium contents of niobium and tantalum in (HF+HCl) solutions at 300 - 550 ° C and 100 MPa in the presence of Co-CoO oxygen buffer. The initial HF concentration varied from 0.01m to 2 m, and the HCl concentration remained constant at 0.5 m. The effect of temperature on the solubility of Ta and Nb oxides, as well as pyrochlore and tantalite minerals, has been established. A comparative analysis of the equilibrium contents of Nb and Ta has been carried out.

Keywords: experiment, tantalite, pyrochlore, tantalum and niobium oxides, solubility, mixed fluoride-chloride solutions

The temperature dependences of the equilibrium contents of Ta and Nb were obtained upon dissolution of niobium (β-Nb_2O_5) and tantalum (β-Ta_2O_5) oxides, as well as natural minerals of pyrochlore $(Ca, Na)_2(Nb,Ta)_2O_6(O, OH, F)$ and tantalite $(Mn, Fe)_2(Ta, Nb)_2O_6$ in solutions of mixed composition (HF + HCl) at 300-550 ° C and 1000 bar (Co-CoO buffer). The initial HF concentration varied from 0.01m to 2m, and HCl concentration remained constant and was 0.5 m. Experiments were performed on a hydrothermal line. A sealed-capsule quench technique was employed. After the run the quenched aqueous solutions were analyzed using ICP/MS (Inductively Coupled Plasma Mass Spectrometry) and ICP/AES (Atomic Emission Spectroscopy) for Nb, Ta, Mn, and Fe and admixture elements Ti, W, and Sn,. The composition of the solid run products was characterized using optical microscopy, X-ray diffraction, and electron microprobe analysis (Cam Scan MV 2300 (VEGA TS5130MM. The solubility of Ta and Nb oxides was

studied using the Ta_2O_5 and Nb_2O_5 reagents which were preliminarily purified by hydrothermal recrystallization in 0.1 *m*HF at 550°C and 1000 bar. In the experiments, we used pyrochlore monocrystals from the weathering crusts of the Tatarka carbonatite deposit having the following composition (wt%):Na_2O 7.61%; CaO 14.28%; Nb_2O_5 71.61; F 5.18; TiO_2 0.83; Ta_2O_5≤1%) and tantalite - from quartz-amazonite-micaceous pegmatoids of the Etykinsky tantalum deposit of composition (wt%): Nb_2O_5 58.99%, Ta_2O_5 17.70%, MnO 13.51%, FeO 4.42%, TiO_2 2.59%, SnO_2 1.54%, WO_3 1.24% (average of seven analyzes) according to the analysis on the CamScan MV2300 electron microprobe (VEGA TS 5130MM). We used the fragments ~2 mm in size cut out of them and weighing 0.1–0.2 g. The crystals were preliminarily treated with 0.1 *m* HF solution, washed with water, and dried. Run duration was 15- 30 days.

The results of the experiments on the solubility of tantalite in (HF + HCl) solutions at 300-550 ° C and 1000 bar (Co-CoO buffer) are presented in **Fig. 1a, b**. Analysis of the data obtained showed that at low fluoride concentrations (0.01m HF + 0.5 m HCl) and (0.1m HF + 0.5 m HCl), the equilibrium tantalum content (**Fig. 1a**) at 300, 500, and 550° C does not exceed 10^{-7} mol / kg H_2O, and at 400°C mTa is even lower. In the region of high HF concentrations: (2mHF + 0.5mHCl), the Ta content in the solution at 300 °C increases to n * 10^{-4} mol / kg H_2O, and at 500 ° C it reaches n * 10^{-2} mol / kg H_2O. At 550 ° C, for all selected concentrations (mHF + 0.5mHCl), the tantalum content is n * 10^{-7} mol / kg H_2O, which is associated with the formation of the solid phase Mn_2TaO_3 in the solution. The temperature dependence of the niobium content upon dissolution of tantalite is shown in **Fig. 1b**. At low fluoride concentrations (0.01m HF + 0.5 m HCl) and (0.1m HF + 0.5 m HCl), the trend of temperature dependence has the same form as for tantalum, but the niobium content is two orders of magnitude higher. At high HF concentrations (1mHF + 0.5mHCl) solution, the inverse temperature dependence is observed: with increasing temperature, the niobium content decreases, while for the (2mHF + 0.5mHCl) solution, it is hardly noticeable. In this case, the niobium content has a maximum value - n * 10^{-1} mol / kg H_2O.

Experimental results of studying the temperature dependence of the equilibrium tantalum content upon dissolution of Ta_2O_5 and tantalite in (0.1mHF + 0.5mHCl) and (1mHF + 0.5mHCl) solutions are shown in **Fig. 2**. For Ta_2O_5, the tantalum content in both solutions is an order of magnitude higher than for tantalite. But at the same time, with increasing temperature the tantalum content is practically independent of temperature. Comparison of the experimental results on the tantalum oxide and natural tantalite solubility in mixed (HF + HCl) solutions has previously shown (Korzhinskaya, Kotova; 2017) that at low fluoride concentrations (0.01m HF + 0.5mHCl) the solubilities of tantalum oxide and tantalite are practically the same. However, with an increase in the HF concentration, the equilibrium Ta content for Ta_2O_5 sharply increases and in (2 m HF + 0.5 m HCl) solution reaches values of 10^{-2} mol / kg H_2O, which is four orders of magnitude higher than that of tantalite.

When Nb_2O_5 is dissolved in (0.1mHF + 0.5mHCl) solution at 300°C **(Fig. 3a)**, the niobium content is 1.5 orders of magnitude higher than that of pyrochlore. A change in temperature has no significant effect on the solubility of niobium oxide in (HF + HCl) solutions, while the positive temperature dependence is observed for pyrochlore and tantalite. In solutions with a high content of the F^- ion (1mHF + 0.5mHCl) (**Fig. 3b**), the niobium oxide solubility increases by 1.5 orders of magnitude

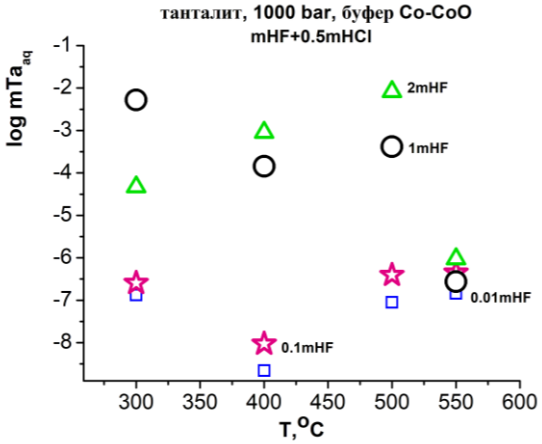

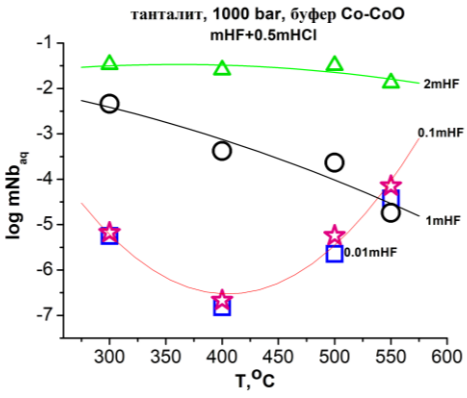

Fig. 1a. Temperature dependence of the equilibrium tantalum content upon dissolution of tantalite in (mHF + 0.5mHCl) solutions (Co-CoO buffer)

Fig. 1b. Temperature dependence of the equilibrium niobium content upon dissolution of tantalite in (mHF + 0.5mHCl) solutions (CO-CoO buffer)

and is $n*10^{-2}$ mol / kg H_2O, which practically coincides with the niobium content upon dissolution of pyrochlore at the same conditions (Korzhinskaya, Kotova, 2016). The increasing temperature has no significant effect on the change in the solubility of minerals.

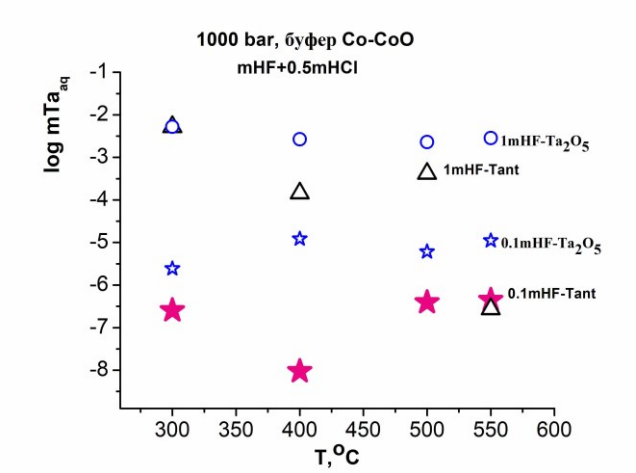

Fig. 2. Temperature dependence of the equilibrium tantalum content upon dissolution of Ta_2O_5 and tantalite in (0.1mHF + 0.5mHCl) and (1mHF+0.5mHCl) solutions (Co-CoO buffer)

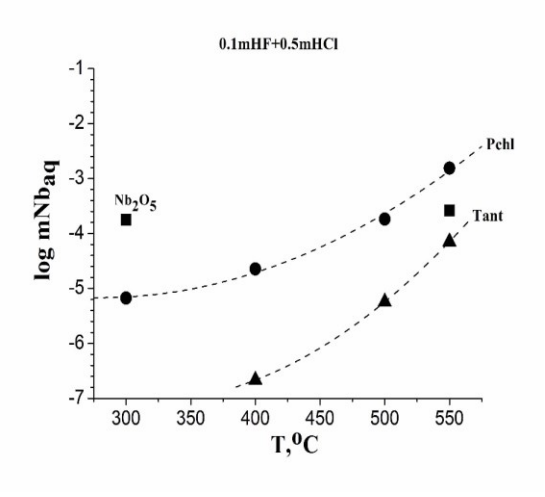

Fig. 3a. Temperature dependence of the equilibrium niobium content upon dissolution of Nb_2O_5, pyrochlore and tantalite in (0.1mHF + 0.5mHCl) solution (Co-CoO buffer)

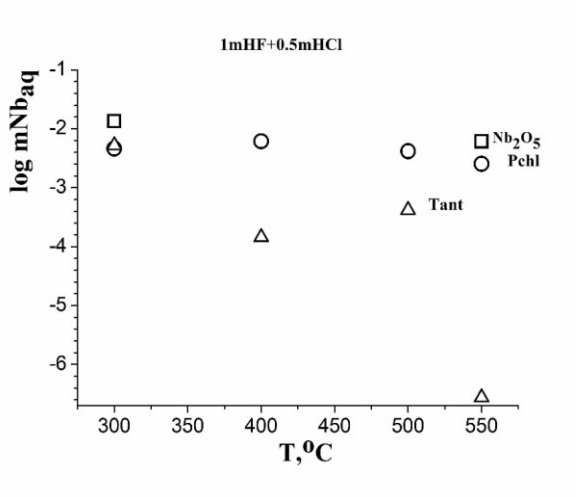

Fig. 3b. Temperature dependence of the equilibrium niobium content upon dissolution of Nb_2O_5, pyrochlore and tantalite in (1mHF + 0.5mHCl) solution (Co-CoO buffer)

The experimental results have shown that the concentrations of Ta and Nb obtained in the study of pyrochlore, tantalite, Ta and Nb oxides solubility in mixed (HF + HCl) fluids are sufficient for real mass transfer of tantalum and niobium by hydrothermal solutions.

This work was supported by the AAAA-A18-118020590151-3 program and the RFBR grant 15-05-03393

References

Korzhinskaya V.S., Kotova N.P. Experimental study of fluid composition (HF+HCl) influence on niobium behavior when dissolving pyrochlore and niobium oxide at T = 550 °C, P = 1000 bar (Co-CoO buffer). In the book: Proceedings of Russian Annual Seminar on Experimental Mineralogy, Petrology and Geochemistry (RASEMPG - 2016). Moscow, 19-20 April, 2016. GEOKHI RAS. p. 132-133.

Korzhinskaya V.S., Kotova N.P. Behavior of niobium and tantalum oxides, pyrochlore and tantalite in mixed aqueous solutions (HF + HCl) at T = 550°C and P = 1000 bar// Experiment in Geosciences, 2017, Volume 23, N 1, p.p.110-111.

Kotelnikov A.R.[1], Damdinov B.B.[2], Damdinova L.B.[2], Bryanskiy N.V.[3], Akhmedzhanova G.M.[1], Suk N.I.[1] Synthetic fluid inclusions in quartz: a check for the adequacy of capture of ore elements. UDC 550.4.02

[1]Institute of Experimental Mineralogy RAS ,
(kotelnik@iem.ac.ru; sukni@iem.ac.ru);
[2]Institute of geology SD RAS (damdinov@mail.ru);
[3]Institute of geochemistry SD RAS (trdigron@yandex.ru)

Abstract. The synthesis of fluid inclusions in quartz was carried out under hydrothermal conditions at 650°C and 2 kbar. PT parameters were selected so that the fluid was in a homogeneous state during the experiment. The experiments were carried out by the method of capturing the fluid phase when healing cracks in specially prepared columns of quartz. The initial composition of the solutions was specified by mixtures of 1 M KCl ± (1 M NaCl) ± (0.1 M $CuSO_4$) ± (0.1 M $ZnCl_2$) ± (0.1 M Ni $(NO_3)_2$) ± (0.1 M Zn $(NO_3)_2$) taken in certain quantities. In the initial solutions, the Cu/K, Zn/K, and Ni/K ratios varied from 0.017 to 0.019. According to preliminary data on the analysis of synthetic fluid inclusions by laser ablation, it was shown that the ratio Cu/K, Zn/K, Ni/K in the captured fluid portions varied from 0.015 to 0.024, which is close to the values specified in the initial solutions.

Keywords: fluid, synthetic fluid inclusions, hydrothermal conditions, ore elements

The study of fluid inclusions (FI) in minerals provides invaluable information on the TPX conditions of mineral- and petrogenesis. One of the main issues in the study of FI is the adequacy of the capture of the mineral-forming fluid: that is, to what extent the composition and phase relationships during the microthermometric study of the fluid in the studied inclusion will reflect the real values. A review of experimental studies on the problem of the adequacy of FI capture is given in (Kotelnikova, 2001). It can be noted that the adequacy of capture for inclusions of systems: water; water – salt; water – carbon dioxide and water – salt – carbon dioxide has been experimentally proven. A more complex issue is post-capture changes in inclusions under the influence of varying TPX parameters. It was shown that the compositions of the FI can change with changes in temperature and pressure. Nevertheless, a thorough study of FI in natural parageneses makes it possible to reliably study the evolution of geological processes. Experimental studies of binary systems H_2O – NaCl; H_2O – CO_2 and ternary system H_2O – CO_2 – NaCl were carried out by different methods: (1) PVT – research; (2) sampling; (3) synthetic fluid inclusions. Knowing the properties of fluids in the H_2O – CO_2 – NaCl system, we can: 1) by studying fluid inclusions by cryo- and thermometry, estimate the salinity of the fluid, its density, and evaluate the composition of the gas and salt components by various methods; 2) in combination with the analysis of parageneses and calculations of mineral-fluid equilibria, it is possible to determine the TP-parameters of the processes of petro- and mineralogenesis, to calculate the compositions of the gas phase; 3) on the basis of the data obtained, to evaluate the evolution of the TPX parameters of various geological processes. The development of modern methods for the study of FI by laser ablation (opening of inclusions and evaporation of the contents) and ICP MS analysis, due to its high sensitivity, makes it possible to determine the content of ore components. However, this method has not yet been verified experimentally. For this purpose, we decided to synthesize artificial FI in quartz in the water – salt system (with the addition of various ore elements). At the same time, for better reliability and interpretation of the results obtained, the synthesis of FI had to be carried out from a homogeneous fluid.

For this, fluid inclusions were synthesized in quartz under hydrothermal conditions at 650°C and a pressure of 2 kbar. The PT parameters were chosen so that the fluid of the H_2O – KCl system was in a homogeneous state during the experiment. The experiments were carried out by the method of trapping the fluid phase during the healing of cracks in specially prepared quartz columns. The dimensions of the pillars were ~ 5x4x20 mm, the weight varied from 400 to 1500 mG. The initial composition of the solutions was set with mixtures of 1M KCl ± (1M NaCl) ± (0.1M CuSO4) ± (0.1M ZnCl2) ± (0.1M Ni$(NO_3)_2$) ± (0.1M Zn$(NO_3)_2$), taken in certain amounts. In the initial solutions, the ratios Cu/K, Zn/K, Ni/K varied from 0.017 to 0.019. The experiments were carried out in gold ampoules 5 mm in diameter and 0.2 mm in wall thickness. For better healing of cracks, amorphous SiO_2 was added to the ampoules in the amount of 10 wt% of the mass of quartz pillars. The duration of the experiments was up to 20 days. After the experiments, the quartz columns were polished and investigated by microthermometry using a Linkam setup. It is shown that the density of inclusions corresponds to the PT parameters of the experiments. The composition of the inclusions was studied by laser ablation, followed by analysis of the vapor phase on a mass spectrometer. Also, the analysis of the final solutions (after the experiments) for the content of Na, K, Cu, Zn, Ni was carried out by the method of atomic absorption on the "Quant" device.

According to preliminary data from the analysis of synthetic fluid inclusions by laser ablation, it was shown that the Cu/K, Zn/K, Ni/K ratios in the captured fluid portions varied from 0.015 to 0.024, which is close to those specified in the initial solutions.

This work was supported by the AAAA-A18-118020590151-3 program.

Reference

Kotelnikova Z.A. Synthetic and natural fluid inclusions as the basis for modeling the regime of volatiles components during petrogenesis. Abstract of doct. dissertation. Moscow. 2001. 42 p.

Kotelnikov A.R.[1], Suk N.I.[1], Kotelnikova Z.A.[1,2], Korzhinskaya V.S. Fluids in equilibrium with silicate substance and problems of ore genesis UDC 550.89:553.062

[1 1]Institute of Experimental Mineralogy (kotelnik@iem.ac.ru);
[2] Institute of Geology of Ore Deposits, Petrography, Mineralogy, and Geochemistry RAS (kotelnik@igem.ac.ru)

Abstract. The interaction of silicate substances with salt solutions at 650-850°C and 1 kbar has been experimentally shown. Changing the pH and chemical composition of the solution is interpreted from the perspective of heterogenization of water-salt systems according to the type: (1) homogeneous fluid → steam + liquid and (2) homogeneous fluid → liquid 1 + liquid 2. Due to hydrolysis by a reaction of the type: $NaCl + H_2O \leftrightarrow NaOH\downarrow + HCl\uparrow$ alkaline and acid components are formed. At the same time, an interphase distribution of acidic and alkaline hydrolysis products occurs, alkaline components enrich the denser phase, while acidic components go into a less dense phase. This results in the appearance of alkaline silicate melts enriched in water and salt components. Alkaline silicate melts formed during fluid heterogenization can extract ore elements (Ta, Nb) from host rocks and transport them to the apical parts of lithium fluoride granite bodies. Our proposed model of the post-magmatic process with the participation of a heterogenizing fluid allows us to understand the formation of ore differences of granite rocks – apogranites.

Keywords: fluid, equilibrium*, fluid-magmatic systems, fluid inclusions, ore genesis*

The role of fluids in endogenous processes is extremely high, it is: (1) transfer of heat and matter in the processes of petrogenesis; (2) participation in mineral reactions; (3) concentration of ore matter; (4) fluid-magmatic interaction.

Fluid is a supercritical aqueous solution, where there is no short-range order in the arrangement of molecules (as in a gas), at the same time its density is high (as in a liquid). In addition, the fluid is practically incompressible (like a liquid). Fluid is a special supercritical state of matter. The field of fluid stability is extremely high: in the temperature range from the first degrees K – up to 10^8 °K (taking into account the stellar matter); for pressure from 0.0001 - 10^3 kbar.

We can classify fluids by their interaction with silicate (or aluminosilicate) phases. On this basis, three groups are distinguished: (1) neutral (gases such as nitrogen, helium and other neutral gases); (2) low active (water, carbon dioxide, their mixtures and some water-salt systems); (3) active fluids (aqueous salts solutions of I and II types).

Let's consider how fluids interact with solids.

(1) Neutral fluids (mixtures of gases, their aqueous solutions) – for them, there is practically no chemical interaction;

(2) low-active fluids (systems $H_2O – CO_2$, H_2O – NaCl) – these fluid systems are characterized by the reactions of hydration – dehydration, carbonatization – decarbonatization: $MgO + H_2O = Mg(OH)_2$; $CaSiO_3 + CO_2 = CaCO_3 + SiO_2$;

(3) active fluids (systems of I and II types), example: $H_2O – KF$; H_2O – NaF. For them, reactions of fluid-mineral interactions with incongruent dissolution of silicates and aluminosilicates are common.

Under certain conditions, systems of low-active fluids can exhibit the properties of active fluids; this will be discussed in more detail later.

The $H_2O – CO_2$ – NaCl system is usually considered as a model fluid system, as it contains the most common fluid components and has the most important properties of such systems.

Let us first consider one-component systems: 1) water; 2) carbon dioxide, and binary: 3) water – carbon dioxide, and 4) water – sodium chloride. The properties of these systems have been studied in detail in the experimental and theoretical works of domestic and foreign researchers.

Type II binary systems are more complex. The difference in the properties of systems of I and II types is determined by the position of the three-phase equilibrium lines (G + L + C) and the critical curve in the TP coordinates. Type I system: the three-phase equilibrium curve (G + L + C) does not cross the critical curve of the system. Type II system: the three-phase equilibrium curve intersects the critical curve of the system. The lower intersection point is usually called the P point, the upper one – the Q point. Hence the name of solutions as PQ-type solutions arose. Thus, systems of II type are characterized by the presence of critical phenomena in saturated solutions; in addition, they have a negative temperature coefficient of solubility at low pressures in the region up to the point P. The position of the solubility curve in PQ-type solutions strongly depends on pressure, which is not typical for type I solutions. As a rule, type II solutions are characterized by the presence of a liquid immiscibility region of the L1 + L2 type above the point P. Ternary systems with the participation of PQ-type binary systems have very complex phase relationships.

The methods for studying the phase relations of fluids are as follows: (1) PVT - research; (2) sampling; (3) synthetic fluid inclusions. The PVT method has been widely used to study the properties of water, carbon dioxide and a number of binary systems, the sampling method is good for studying the phase compositions, at the same time, both of these methods are limited in PT parameters (limiting temperatures of 550°C and pressures up to 5 kbar). The method of synthetic fluid inclusions (in quartz) allows one to study phase equilibria by the method of direct visual observation, in addition, under certain conditions, it is possible to determine the

compositions of coexisting phases. This method is also promising in the sense that the fluid (similar to natural systems) is always in the presence of a silicate substance (quartz) and the resulting phase relationships can be directly applied to mineral equilibria. Knowledge of the properties of fluid-salt systems, determined by the experimental method, allows one to quantitatively study the evolution of geological processes. Based on the properties of fluids in the H_2O – CO_2 – NaCl system, we can: 1) by studying fluid inclusions by cryo- and thermometry, estimate the salinity of the fluid, its density, and evaluate the compositions of the gas and salt components by various methods; 2) based on the analysis of parageneses, it is possible to determine the TP-parameters of the processes of petro- and mineralogenesis; calculate the composition of the gas phase in equilibrium with minerals; 3) study the evolution of TPX parameters of petrogenesis on the basis of the data obtained.

During the interaction of active fluids (in particular, aqueous solutions of alkali metal fluorides) with a silicate substance, phases of "heavy fluids" saturated with silicate substance are formed. Thus, in the simplest case, we pass from binary systems water – salt to ternary systems water – salt – silicate phase. Often in such systems, fluid immiscibility appears, and hydrolysis reactions are activated with the separation of alkaline and acid components between the immiscible phases of the fluid.

The interaction of a silicate substance with salt solutions at 650-850°C and a pressure of 1 kbar has been shown experimentally. The change in pH, the chemical composition of the solution is interpreted from the standpoint of the heterogenization of water-salt systems by the type: (1) homogeneous fluid → vapor + liquid and (2) homogeneous fluid → liquid 1 + liquid 2. Due to hydrolysis by a reaction like: NaCl + H_2O ↔ NaOH↓ + HCl↑ alkaline and acidic components are formed. At the same time, there is an interphase distribution of acidic and alkaline hydrolysis products. In this case, alkaline components enrich a denser phase, while acidic ones go into a less dense phase, for example, into a vapor phase in equilibrium fluid → vapor + liquid. Due to alkalization, the dense phase reacts with silicate material, causing it to melt according to the mechanism of "metasomatism as magmatic replacement" according to D.S. Korzhinsky. This gives rise to alkaline silicate melts, enriched with water and salt components.

Under natural conditions, a similar mechanism is realized during the intrusion and differentiation of granites with separation of Li-F satellites of granite bodies. The alkaline silicate melts formed during heterogenization of fluids can extract ore elements (Ta, Nb) from the host rocks and transport them to the apical parts of lithium-fluoride granite bodies. During crystallization, these melts form parageneses of feldspar – quartz – ore mineral (tantalum-niobate). The proposed model of the postmagmatic process with the participation of a heterogenizing fluid makes it possible to understand the formation of ore varieties of granite rocks – apogranites.

In general, the heterogenization of fluid-silicate (magmatic) systems with a decrease in pressure (in the course of the evolution of geological systems) can be the most important factor in the concentration of ore matter and the processes of ore genesis.

This work was supported by the AAAA-A18-118020590151-3 program and the RFBR *grant 15-05-03393.*

Redkin A.F. Tungsten valence in hydrothermal solutions on the experimental and calculated data.

Institute of Experimental Mineralogy RAS (IEM RAS), Chernogolovka, Moscow District, Russia (redkin@iem.ac.ru)

Abstract. The influence of $f(O_2)$, acidity (mHCl) and $CaCl_2$ concentration on $CaWO_4$ solubility at 400 and 500°C, 100 MPa is considered. Model calculations are made at $f(O_2)$, corresponding to NNO and HM buffers, mHCl and $m$$CaCl_2$ from 0.001 to 1.0 mol·kg^{-1} H_2O. Calculations have shown that the solubility of scheelite is influenced by all considered physical and chemical parameters, and the predominant species of tungsten are complexes W(V), with a subordinate number of hydroxo-complexes W(VI).

Keywords: *scheelite, ferberite, solubility, tungsten species, valence, thermodynamic simulations*

The main industrial minerals of tungsten are scheelite $CaWO_4$, wolframite $(Fe,Mn)WO_4$ and its minals are ferberite $FeWO_4$, hubnerite $MnWO_4$. The formation of certain ores is primarily associated with the features of the host rocks. Thus, the deposition of scheelite is facilitated by calcium-containing rocks (skarns, marbled limestones), while wolframite is formed in the process of greisenization of granite rocks. Scheelite and scheelite-wolframite deposits are formed at the greysen and skarn contacts. It is generally accepted that the transfer of tungsten by hydrothermal solutions is carried out in the form of W(VI) species: WO_4^{2-}, HWO_4^-, and $H_2WO_4^0$ (Ivanova, Khodakovsky,1968; Ivanova, 1972), $NaWO_4^-$ (Wood, Samson, 2000). The role of polymer species W(VI) decreases with increasing temperature according to (Wesolowski et al., 1984), and the formation of silicic-12-tungstic acid and its salts (Orlov et al., 2000) is not experimentally justified. Tungsten halide complexes (Veispäls, 1979, Galkin, 1985; Bryzgalin, 1976; Khodarevskaya et al., 1990) may probably be present, but their role in ore Genesis is secondary (Bychkov, Matveeva, 2008).

We experimentally studied the solubility of synthetic ferberite $FeWO_4$ at 400-500°C, pressure 20, 25, 40, 50 and 100 MPa, $f(O_2)$ corresponding to Ni-NiO (NNO), Fe_3O_4-Fe_2O_3 (HM) buffers, in solutions containing 0.7 ÷ 8.9 *m*KCl, and acidity controlled by a Quartz-Microcline-Muscovite buffer. It was found that *m*W depends on *m*Cl, *T* and $f(O_2)$ and varies from $1 \cdot 10^{-4}$-0. 05 mol·kg^{-1} H_2O in 0.7 *m*KCl to 0.01-0.15 mol·kg^{-1} in 8.9 *m*KCl. (Redkin, Cygan, 2020). Thermodynamic calculations performed at *P*=100 MPa showed that the predominant tungsten species in solutions of KCl-HCl and $f(O_2) = fO_2$ (NNO) could be W (V, VI) species: WO_3^-, HWO_4^-, $H_2W_2O_7^-$ at 500°C and HWO_4^-, $W_5O_{16}^{3-}$ at 400°C.

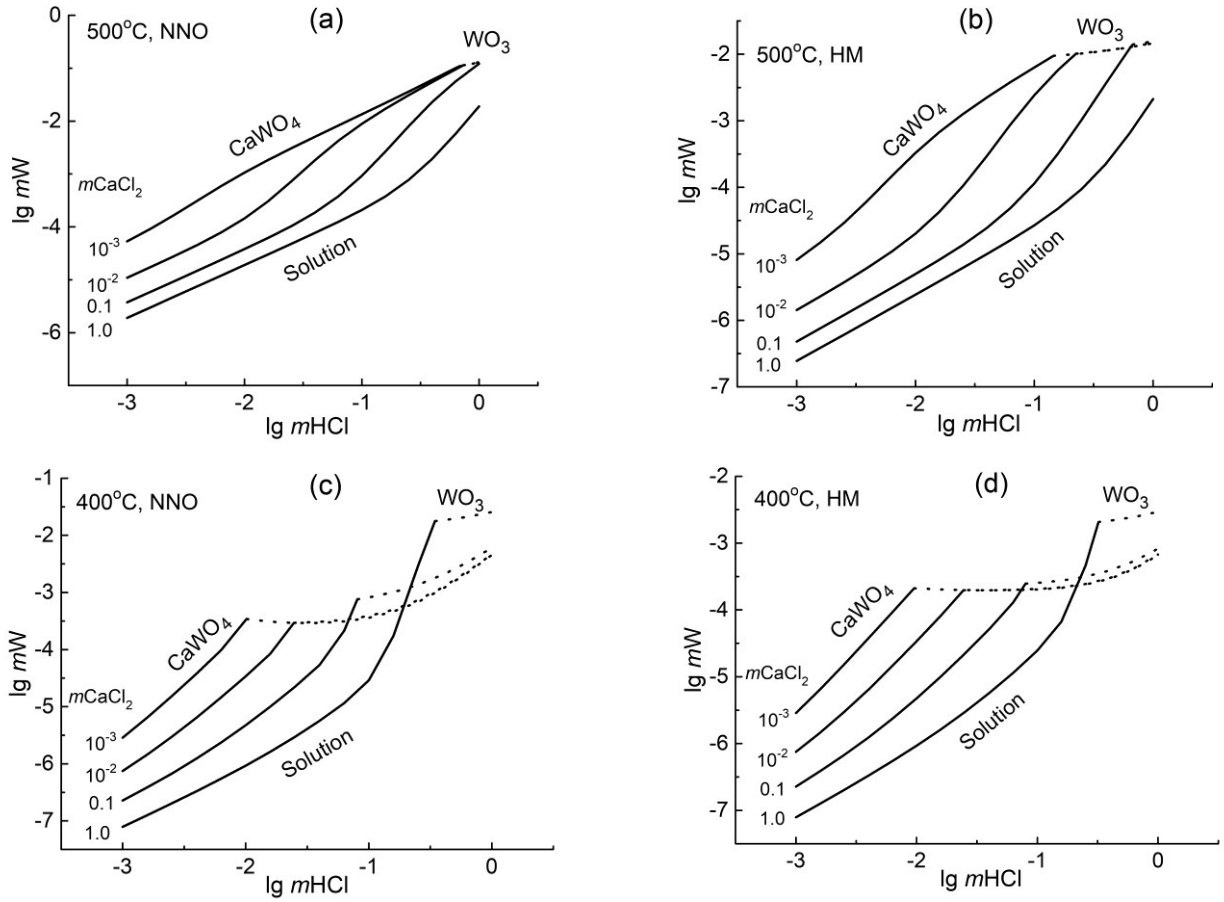

Fig. 1. Results of modeling the solubility of scheelite in chloride solutions of $CaCl_2$-HCl at 400-500°C, 100 MPa and $f(O_2)$ corresponding to NNO and HM buffers.

Despite the fact that we have already proposed possible forms of W(V) transfer, their role requires experimental justification. The most important ore mineral – scheelite (Sch) was chosen as the object for research. In this mineral, there is only one element, tungsten, that can change the valence during the transition from the mineral to the solution. In this paper, the influence of $f(O_2)$, acidity (*m*HCl) and $CaCl_2$ concentration on the solubility of $CaWO_4$ at 500 and 400°C, 100 MPa is considered. Model calculations (Fig. 1) were performed for $f(O_2)$ corresponding to NNO and HM buffers, *m*HCl and *m*$CaCl_2$ from 10^{-3} to 1.0 mol kg^{-1} H_2O. Calculations have shown that the solubility of scheelite is influenced by all the considered physical and chemical parameters. An increase in the concentration of calcium in the solution (*m*$CaCl_2$) and $f(O_2)$ reduces mW_{total}, while an increase in temperature and *m*HCl increases the content of tungsten in the solution. The predominant complex species of tungsten are W(V) complexes, with a subordinate number of W(VI) hydroxocomplexes. The increase in the content of charged species in a solution in equilibrium with scheelite is mainly influenced by the ionic strength of the solution. As the ionic strength of the solution increases, the activity coefficients of charged species decrease, and the concentrations of these species increase. For experimental studies, solutions of $CaCl_2$-HCl-H_2O containing $m\text{HCl}>10^{-2}$ and $m\text{CaCl}_2<10^{-2}$ in which $m\text{W}>10^{-4}$ are of interest. However, in solutions enriched with HCl, there is an incongruent solubility of Sch with the formation of WO_3 (region of $+WO_3$ in Fig. 1). Fig. 2 shows the expected concentrations of tungsten in equilibrium with the Sch+WO_3 assemblage at 400-500°C, 100 MPa. According to calculations, the increase in HCl concentration at 500° and given $f(O_2)$ has very little effect on *m*W. At 400°C this effect is noticeably greater, but at

mHCl>0.1 mol·kg^{-1}. This is primarily due to the charge of the predominant particle ($W_5O_{16}^{3-}$).

The calculations have shown that when planning experiments on solubility, both physical and chemical parameters and the possibility of formation of other phases must be taken into account.

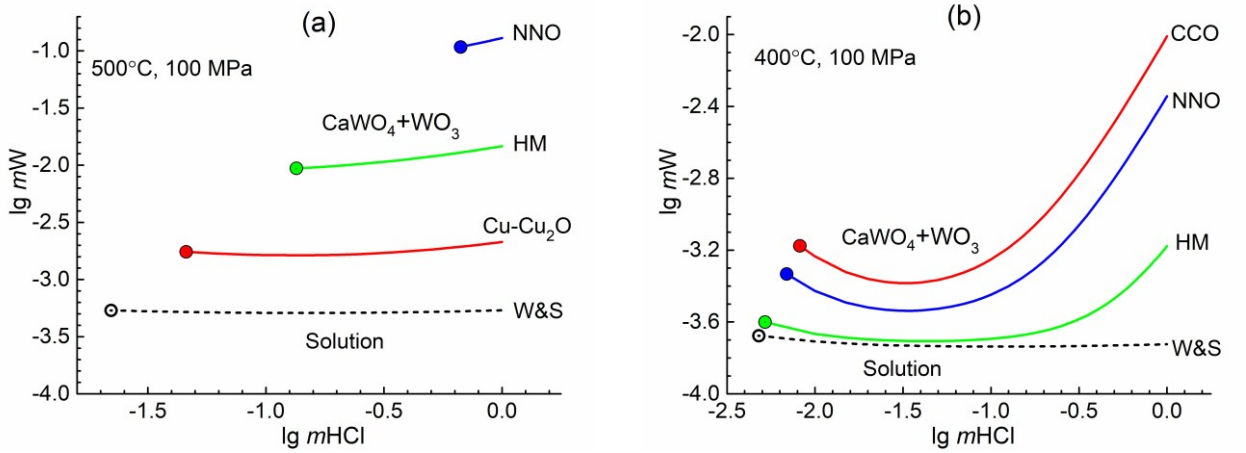

Fig. 2. Results of modeling the incongruent solubility of scheelite with the formation of WO_3 in HCl solutions (initial mCaCl$_2$=0) at 500°C (a) and 400°C (b), 100 MPa and f(O$_2$) corresponding to CCO (Co-CoO), NNO, HM and Cu-Cu$_2$O buffers. W&S-data calculation by (Wood, Samson, 2000).

The work was supported by RFBR grant 20-05-00307 and GZ No AAAA-A18-118020590151-3.

References

Bryzgalin O. V. (1976) Geochemistry of tungsten in the hydrothermal process. M: Nauka. 73 p. (in Russian).

Bychkov A. Yu., Matveeva S. S. (2008) Thermodynamic model of ore bodies formation in the wolframite vein -greisen type Deposit of Akchatau. Geochemistry. No. 9. P. 934-954. (in Russian).

Galkin A.V. (1985) solubility of W-Fe-Mg minerals in high-temperature chloride solutions. PhD thesis. Novosibirsk: IG&G SO of AS USSR. 17 p. (in Russian).

Ivanova G. F., Khodakovsky I. L. (1968) Forms of tungsten migration in hydrothermal solutions. Geochemistry, No. 8, Pp. 930-940. (in Russian).

Ivanova G. F. (1972) Geochemical conditions of formation of wolframite deposits. Moscow: Nauka. 149 P. (in Russian).

Khodarevskaya L. I., Tikhomirova V. I., Postnova L. E. Studying of the solubility of WO3 in HCl solutions at 450°C. DAN SSSR. T. 314. No. 3. P. 720-722. (in Russian).

Orlov R. Yu., Tamm M. E., Vigasina M. F. (2000) 12-wolframphosphate - a possible form of tungsten migration in a hydrothermal medium. Geochemistry, Vol. 38, No. 11, Pp. 1240-1243. (in Russian).

Redkin A.F., Cygan G.L. (2020) Experimental determination of ferberite solubility in the KCl-HCl-H2O system at 400-500 °C, and 20-100 MPa. In book: Advances in Experimental and Genetic Mineralogy (Ed.: Yu. Litvin & O. Safonov). Springer. 137-162.

Veispäls A. (1979) Thermodynamic investigations of the chemical transport of tungsten trioxide. Izvestiya Latv. Acad. Sci., Seriya of Phys. Tech. Sci. 1. 60-65.

Wesolowski D., Drummond S.E., Mesmer R.E., Ohmoto H. (1984) Hydrolysis equilibria of tungsten (VI) in aqueous chloride solution to 300 oC. Inorg.Chem. 23. 8. 1120-1132.

Wood S.A. and Samson I.M. (2000) The hydrothermal geochemistry of tungsten in granitoid environments: I. Relative solubilities of ferberite and scheelite as a function of T, P, pH, and mNaCl. Econ. Geol. 95. 143-182.

Sidkina E.S.[1], Mironenko M.V.[1], Polyakov V.B.[2] Calculation of serpentinization of olivin. Verification of the equilibrium-kinetic model.

[1] GEOKHI RAS, Moscow (sidkinaes@yandex.ru, mikhail_mironenk@mail.ru)

2 IEM RAS, Chernogolovka Moscow district (vpolyakov@mail.ru)

Abstract. We calculated reaction flow in the closed system "0.495 M NaCl and 0.0194 M $NaHCO_3$ aqueous solution + olivine (Fo91)" at temperatures 200 ºC and 320ºC and pressure 350 bar. The water/rock ratio, temperatures and pressure, the chemical composition and grain size of olivine, the chemical composition of aqueous solution, as well as duration of interactions were the same as in the experiments, described in (McCollom et al., 2016; McCollom, 2016). The results of calculations were compared with experimental results. The newly formed mineral assemblage in both cases consisted of high-magnesian serpentine and brusite, magnetite, and of a small amount of magnesite at 200ºC. The calculated rate of olivine serpentinization was close to the experimentally observed rate.

Keywords: methane synthesis, hydrogen, sea water, equilibrium-kinetic modeling, carbon isotopes fractionation

The model experiments on olivine serpentinization, described in detail in (McCollom et al., 2016; McCollom, 2016), gave a possibility to verify the equilibrium-kinetic model, which was developed on the basis of the complex

GEOCHEQ_M. In our model the rate of serpentinization is determined by the rate of congruent dissolution of olivine. A chemical reaction of olivine with sea water results in formation of chrysotile, brucite, and magnetite and can be written in simplified form as

$(Mg,Fe)_2SiO_4 + H_2O \rightarrow Mg_3Si_2O_9(OH)_4 + Mg(OH)_2 + + Fe_3O_4 + H_2$

Methane may form as a result of interaction of hydrogen with inorganic carbon of sea water:

$4H_2+CO_2 = CH_4 + 2H_2O$

The model description The equilibrium-kinetic model of irreversible chemical interaction in systems "aqueous solution-rock" is described in (Mironenko and Zolotov, 2012; Zolotov and Mironenko, 2007). The model had been developed on the basis of the complex GEOCHEQ_M (Mironenko et al., 2008) A thermodynamic data base is based on the well-known data base SUPCRT92 (Johnson et al., 1992) with numerous additions. The data base also contains values of kinetic parameters for calculating rates of congruent dissolution of most important silicates, aluminosilicates, oxides, and hydroxides at 25ºC depending on pH, as well as activation energies of these reactions.

For numerical reproducing experiments on olivine serpentinization, we added some missing thermodynamic information. As we needed to take into account formation of Fe-containing brucite, data on thermodynamic properties of amakinite $Fe(OH)_2$ from (Iorish et al., 1978-2004) were used. Besides, because the most realistic, on our mind, descriptions of kinetics of olivine (Fo91) and brucite dissolution do not correspond to formats of GEOCHEQ_M data base, dissolution rates r of these minerals have been calculated using individual formulas

(for olivine $\lg \quad r(pH,T) = lgA - \frac{E_A}{2.303R}\left(\frac{1}{T}\right) - n \cdot pH, lgA = 0.54 \pm 0.14, E_a = 42.6 \pm 0.8 \frac{kJ}{mol}, n = 0.5 \pm 0.004$ from (Rosso and Rimstidt, 2000), and

for brucite $r = A_a exp\left(E_a/_{RT}\right)\left(\frac{a^2_{H+}}{a^2_{H+}}\right)^{1/8}, A_a = 1.7 \cdot 10^{-3}$ mol cm^{-2} sec^{-}, $E_A = 46$ kJ/mol from (Declerq and Oekers, 2014)).

The model must consider a possibility of formation of solid solutions of variable composition. We need to distinguish solid solutions of any mineral, formed or dissolved at different time intervals. For this goal, potential solid solutions Mg-Fe serpentine and Mg-Fe brucite were considered as series of discrete minerals with fixed formulae, which differ from each other by 0.002 stoichiometric units. Free energies of these intermediate members were calculated using the model of ideal mixture. Isomorphic entering of Fe(III) into serpentine was not considered. For calculating fractionation of carbon isotopes among possible magnesite, siderite, and aqueous solution we also used ideal solid solutions of isotopologues of magnesite $Mg(^{12}C,^{13}C)O_3$ and siderite $Fe(^{12}C,^{13}C)O_3$, but we supposed that isotopic re-equilibration took place during deposition of these minerals at each time step.

For simultaneous calculation of chemical and carbon isotopic equilibria by Gibbs free energy minimization method, we modified the data base GEOCHEQ (Mironenko et al. 2000) into GEOCHEQ_Isotope data base (Mironenko et al., 2018) by addition the isotope ^{13}C as a new independent component (chemical element). Accordantly, we added into the list of substances rare isotopologues of the most important C-containing compounds. β-factors of these compounds were critically evaluated and adjusted (Mironenko et al., 2018). It gives possibility to calculate Gibbs free energies of rare isotopologues. Since the values of β-factors of dissolved $^{13}CH_4$,aq, $^{13}C_2H_6$,aq, $^{13}C_3H_8$,aq are unknown, we took β-factors of corresponding gases.

Combination of data from GEOCHEQ_M and GEOCHEQ_Isotope data bases gave possibility to form a dataset for equilibrium-kinetic modeling of hydrothermal serpentinization, taking into account carbon isotope fractionation.

We numerically reproduced experiments (McCollom et al., 2016) at temperature of 200ºC (duration 3331 hours) and at 320ºC (duration 2087 hours). Pressure in both cases was 350 bar. Aqueous solution of 0.495 M NaCl and 0.0194 M $NaH^{13}CO_3$, imitating seawater, was added to fraction of 53-212 μm of olivine Fo_{91} (a chemical composition approximately corresponds to $Mg_{1.82}Fe_{0.18}SiO_4$). The W/R ratio is equal to 2.55. Calculated values of pH of the solution are 7.87 for 200ºC and 8.50 for 320ºC respectively. As opposed to experiments, for modeling we took initial isotopic composition of soda $^{13}C/^{12}C=0.0112372$ ($\delta^{13}C=0$ respectively the standard PDB (see for example, Galimov, 1968)). For initial sample we calculated surface area of spherical grains of olivine of diameter of 132.5 μm (the arithmetic mean between 53 and 212). In the experiment surface area had been determined experimentally by the conventional BET method with N_2 as the adsorptive species. The surface area was found to be 0.59± 0.02 m^2 g^{-1}.

Comparison of the results of computer modeling with experiments. Calculated mineral transformations during serpentinization at 200 and 320ºC are shown in fig. 1. Total amounts of dissolved olivine during interaction are close to experimental ones for both temperatures (figures 1a, 1d). This confirms adequacy of our model and correctness of parameters of the kinetic equation for

Fo_{91} dissolution. Secondary mineral assemblages correspond to experimental ones: high-Mg serpentine, magnetite, and brucite (fig. 1b, 1d).

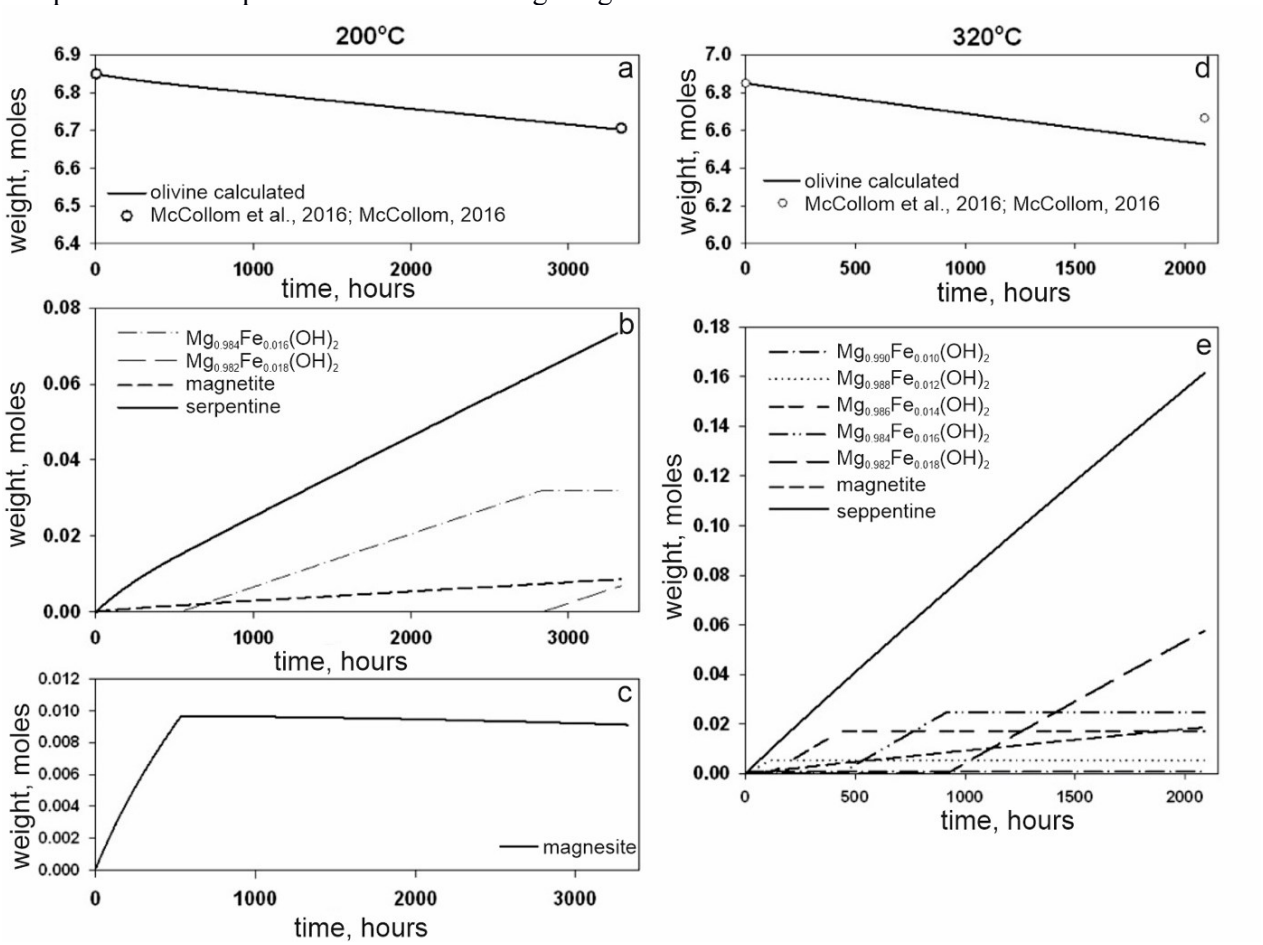

Fig. 1. Calculated masses of dissolving olivine (a,d); masses of newly formed serpentine and magnetite, masses and chemical compositions of brucite (b, e); mass of magnetite (c) for 200 and 320ºC in time.

According to calculations, for 200ºC, at the beginning of interactions, a small amount of magnesite forms. Thereafter it dissolves a little and brucite precipitates. In (McCollom et al., 2016) the presence of small amounts of carbonate was noted in most experiments (Fig 4d, McCollom et al., 2016), but rigorous checking of the results of the experiments with olivine at 320º did not find it.

The calculated composition of serpentine is higher in magnesium (99 mol%) than in experiments (97-96 mol%) and demonstrates constancy regardless temperature and degree of olivine serpentinization.

In our calculations for 200ºC, formation of brucite starts after ending of magnesite deposition, approximately 540 hours after the beginning of interactions. At 320ºC brucite begins to precipitate within the first hour of interactions. Calculated magnesium content in brucite, in contrast to serpentine, varies within the range of 98.7 – 99 mol% (92-99 mol% in experiments). At that time, as well as in experiments (Fig. 5, McCollom et al., 2016), Fe content is higher at lower temperature, besides it gradually increases during serpentinization progress (fig. 1b, 1d).

Calculated concentrations of methane and hydrogen in fluid for 200º are shown in fig. 2b, 2d. At 200º methane concentrations significantly exceed hydrogen contents, for 320º hydrogen dominates. In fact, methane is only hydrocarbon, formed in the system; calculated molalities of dissolved ethane and propane are about $7 \cdot 10^{-9}$ and $5 \cdot 10^{-13}$ for 200ºC, and $5 \cdot 10^{-10}$ and $1 \cdot 10^{-13}$ for 320ºC. Calculated acidity of fluid is shown in fig. 2a, 2c. For 200º after magnesite deposition, pH slightly increases from 8.35 to 8.39. For 320º pH gradually increases from pH=8.50 to 8.54 during interactions.

Calculated fractionation of carbon isotopes between fluid species and magnesite for 200ºC is shown in fig. 3. At the beginning (from 0 to 535 hours, fig. 1c) magnesite deposits. At this stage a minor, but consistent enrichment with ^{13}C of magnesite and dissolved inorganic carbon, takes place. This is due to formation of methane, depleted with this isotope. For the second stage we postulated the absence of isotopic fractionation during congruent dissolution of magnesite. This postulate had been justified in (Polyakov, 1989). Thus, at the second stage (after 535 hours) an isotopic composition of magnesite did not change.

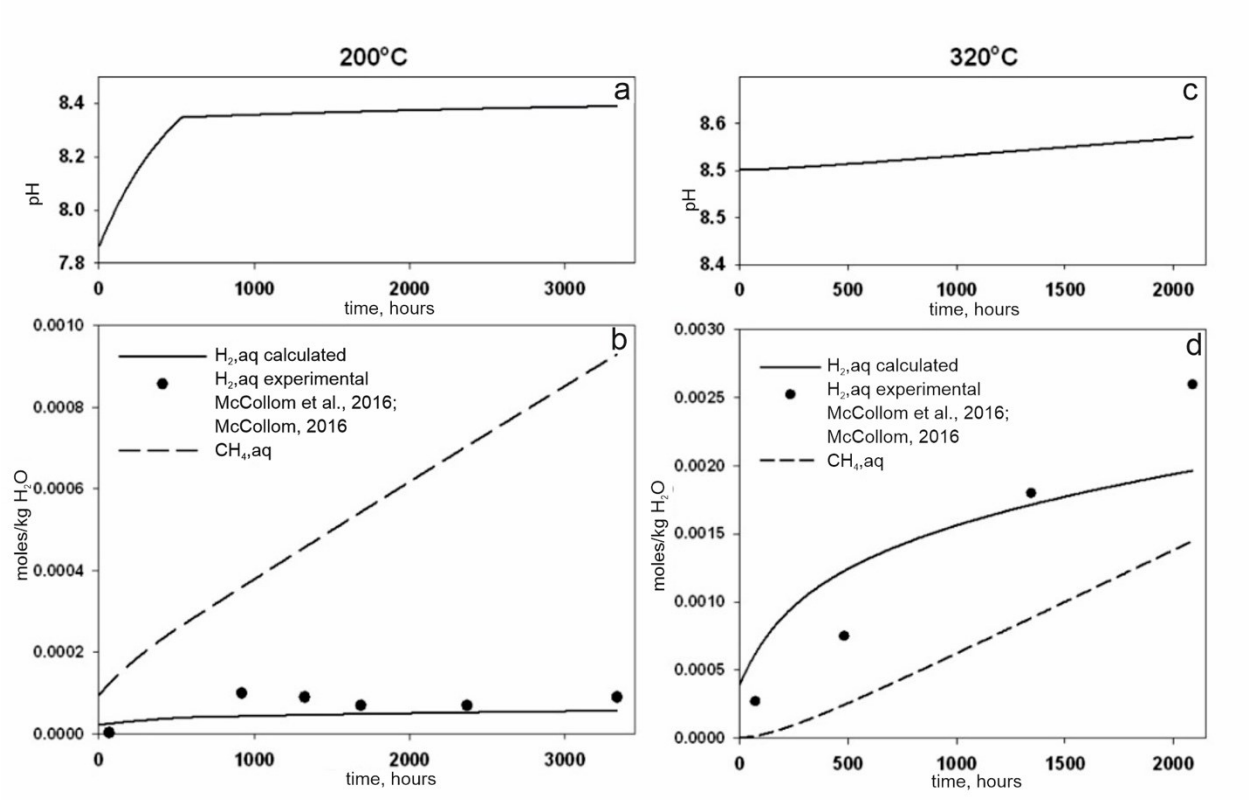

Fig. 2. Calculated changes in pH (a, c); concentrations of hydrogen and methane (b,d) for 200º and 320ºC in time in the system with methane formation.

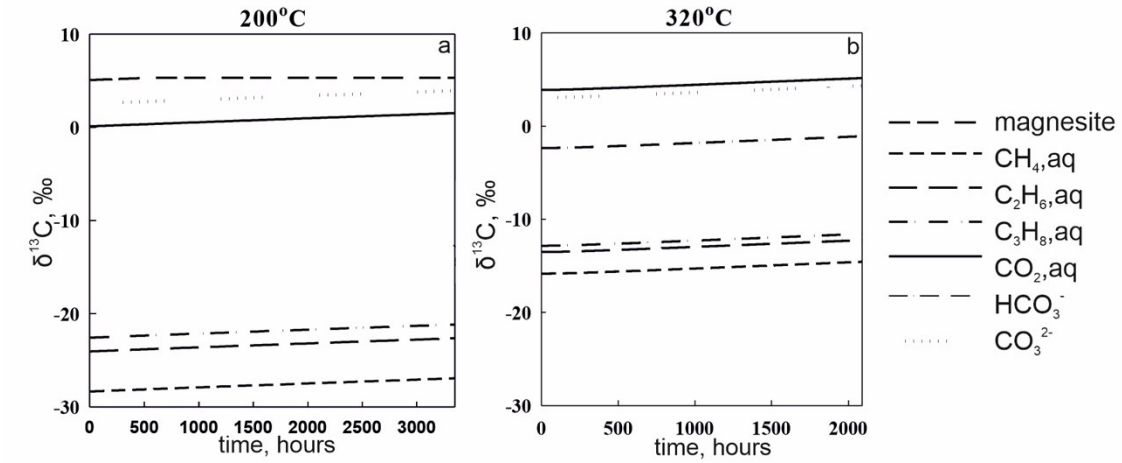

Fig. 3. Calculated fractionation of carbon isotopes among fluid species and magnesite for 200ºC (a) and among fluid species for 320ºC (b)

At 320°C magnesite does not form (fig. 3b). Isotopic composition of dissolved inorganic matter gradually enriches with the heavy isotope (from $\delta^{13}C$ = 0 ‰ to $\delta^{13}C$ = 1.5 ‰) due to formation of methane with low values $\delta^{13}C$ (from -15.8 to -14.6 ‰).

Conclusions

Our attempt numerically, using equilibrium-kinetic model, to reproduce the results of the described in detail experiments on olivine serpentinization showed, that the model satisfactorily reproduced rates of olivine corrosion and secondary mineral formation, chemical compositions of mineral solid solutions, and hydrogen generation.

Experimental investigations has shown, that the chemical reaction of methane synthesis from inorganic matter and hydrogen has hard kinetic constrains and flows very slow in absence of specific catalysts (Horita and Berndt, 1999; Charlou et al.,2010). We did not kinetically restrict the synthesis of methane. Our results agree with field data (Delacour et al., 2008; Proskurowski et al., 2008). At

the same time calculated fractionation of carbon isotopes at equilibrium methane synthesis is comparable with measured fractionation in natural fluids.

Aknowledgment. The study was supported by Russian Foundation for Basic Reseach, grant 19-05-00865a

References

Galimov E.M. (1968) Geochemistry of stable isotopes of carbon. Nedra. 226P. In Russian.

Iorish V.S., Aristova N.M., Bergman G.A., Gorokhov L.N., Gusarov A.V., Ezhov Yu.S., Kulikov A.N., Osina E.L., Sheniavsraya E.A., Khandamirova N.E., Yungman V.S. (1978-2004). Thermodynamic properties of individual substances. Nauka. V.5. Nable 2080. In Russian

Mironenko M.V., Zolotov M.Yu. (2012) Equilibrium-kinetic model of water-rock interaction. *Geochemistry International.* V.50. N 1.1-7.

Mironenko M. V., Akinfiev N. N., Melikhova T. Yu."GEOSHEQ—Complex for Thermodynamic Modeling of Geochemical Systems," Vestn. OGGGGN Ross.Akad. Nauk 5 (15), (2000). URL: http:www.scgis.Ru/Russian/cp1251/H_dggms/5_2000/Term, 10.

Polyakov V.B. (1989) Diffusion-limited isotope effect in a heterogeneous reaction in the kinetic regime. Theory. Chemical physics. T.8., 11. 1539-1541. In Russian

Charlou J.L., Donval J.P., Konn C., Ondréas H., Fouquet Y. (2010) High production and fluxes of H_2 and CH_4 and evidence of abiotic hydrocarbon synthesis by serpentinization in ultramafic-hosted hydrothermal systems on the Mid-Atlantic Ridge. Diversity of Hydrothermal Systems on Slow-Spreading Ocean Ridges, eds. Rona P, Devey C, Dyment J, Murton B. Washington, DC: American Geophysical Union, 265–296.

Declercq J., Oelkers E.H. (2014) CarbFix Report PHREEQC mineral dissolution kinetics database. Geoscience Environement Toulouse, 197 p.

Delacour A., FruËh-Green G. L., Bernasconi S. M., Schaeffer Ph., Kelley D. S. (2008) Carbon geochemistry of serpentinites in the Lost City Hydrothermal System (30_N, MAR). *Geochim. Cosmochim. Acta* **72,** 3681–3702.

Johnson J.W., Oelkers E.H., Helgeson H.C. (1992) SUPCRT92: A software package for calculating the standard molal thermodynamic properties of minerals, gases, aqueous species, and reactions from 1 to 5000 bar and 0 to 1000°C . *Computers & Geosciences* **18** (7), P. 899-947.

McCollom T. M., Klein F., Robbins M., Moskowitz B., Berquor T. S., JoËns N., Bach W., Templeton A. (2016) Temperature trends for reaction rates, hydrogen generation, and partitioning of iron during experimental serpentinization of olivine. *Geochim. Cosmochim. Acta* 181, 175–200.

McCollom T. M. (2016) Abiotic methane formation during experimental serpentinization of olivine. *Proc. Natl. Acad. Sci. USA* **113** (49), 13965-13970.

Mironenko M.V., Polyakov V. B., and Alenina M. V. (2018) Simultaneous calculation of chemical and isotope equilibria using the GEOCHEQ_Isotope software: carbon isotopes. *Geochem. Int.* **56** (13), 1354–1367.

Proskurowski G, et al. (2008) Abiogenic hydrocarbon production at Lost City hydrothermal field. *Science* **319**(5863), 604–607.

Rosso J.J. and Rimstidt J.D. (2000) A high resolution study of forsterite dissolution rates. *Geochim. Cosmochim. Acta* **64** (5), 797–811.

Zolotov, M. Yu., and Mironenko, M. V. (2007) Timing of Acid Weathering on Mars: A Kinetic-Thermodynamic Assessment. *J. Geophys. Research, [Planets]* **112** E07006, doi:10.1029/2006JE002882